Aquat Geochem (2016) 22:469–504
DOI 10.1007/s10498-016-9301-7

ORIGINAL ARTICLE

The Influence of Bioturbation on Iron and Sulphur Cycling in Marine Sediments: A Model Analysis

Sebastiaan van de Velde[1] · **Filip J. R. Meysman**[1,2]

Received: 23 January 2016 / Accepted: 24 August 2016 / Published online: 10 September 2016

Abstract The geochemical cycles of iron and sulphur in marine sediments are strongly intertwined and give rise to a complex network of redox and precipitation reactions. Bioturbation refers to all modes of transport of particles and solutes induced by larger organisms, and in the present-day seafloor, bioturbation is one of the most important factors controlling the biogeochemical cycling of iron and sulphur. To better understand how bioturbation controls Fe and S cycling, we developed reactive transport model of a coastal sediment impacted by faunal activity. Subsequently, we performed a model sensitivity analysis, separately investigating the two different transport modes of bioturbation, i.e. bio-mixing (solid particle transport) and bio-irrigation (enhanced solute transport). This analysis reveals that bio-mixing and bio-irrigation have distinct—and largely opposing effects on both the iron and sulphur cycles. Bio-mixing enhances transport between the oxic and suboxic zones, thus promoting the reduction of oxidised species (e.g. iron oxyhydroxides) and the oxidation of reduced species (e.g. iron sulphides). Through the reoxidation of iron sulphides, bio-mixing strongly enhances the recycling of Fe and S between their reduced and oxidised states. Bio-irrigation on the other hand removes reduced solutes, i.e. ferrous iron and free sulphide, from the sediment pore water. These reduced species are then reoxidised in the overlying water and not recycled within the sediment column, which leads to a decrease in Fe and S recycling. Overall, our results demonstrate that the ecology of the macrofauna (inducing bio-mixing or bio-irrigation, or both) matters when assessing their impact on sediment geochemistry. This finding seems

Electronic supplementary material The online version of this article (doi:10.1007/s10498-016-9301-7) contains supplementary material, which is available to authorized users.

✉ Sebastiaan van de Velde
sevdevel@vub.ac.be

[1] Department of Analytical, Environmental and Geo-Chemistry, Vrije Universiteit Brussel (VUB), Pleinlaan 2, 1050 Brussels, Belgium

[2] Department of Ecosystem Studies, The Royal Netherlands Institute of Sea Research (NIOZ), Korringaweg 7, 4401 NT Yerseke, The Netherlands

particularly relevant for sedimentary cycling across Cambrian transition, when benthic fauna started colonizing and reworking the seafloor.

Keywords Reactive transport modelling · Diagenetic cycling · Iron · Sulphur · Bioturbation · Bio-mixing · Bio-irrigation

1 Introduction

The biogeochemical cycles of iron and sulphur in marine sediments are closely coupled, both in the present-day ocean and in the geological past (Raiswell and Canfield 2012). Foremost, both sulphate and iron (oxyhydr)oxides are used as electron acceptors in the oxidation of sedimentary organic matter in the seafloor (Zobell and Rittenberg 1948; Lovley 1991). While sulphate reduction is considered to be the most important anaerobic mineralization pathway in coastal and shelf sediments (Jørgensen 1982), dissimilatory iron reduction can be important in sediments that combine a strong iron (oxyhydr)oxide input with active bioturbation (Canfield et al. 1993).

The principal reaction products of dissimilatory iron reduction and sulphate reduction are ferrous iron and free sulphide, respectively, and these reduced compounds can subsequently engage in a number of biogeochemical transformations, which often results in a close coupling of the iron and sulphur cycles. In the presence of oxygen, ferrous iron and free sulphide are quickly reoxidised back to sulphate and fresh ferrihydrite (Millero et al. 1987a, b), while in deeper sediment horizons, free sulphide can also be oxidised by iron(oxyhydr)oxides (Canfield 1989; Poulton et al. 2004b). Furthermore, when present at the same location in the pore water, ferrous iron and free sulphide will precipitate almost instantaneously as iron monosulphide (FeS) (Rickard 2006), which is typically a precursor for pyrite (FeS_2) (Rickard and Luther 2007). Both FeS and FeS_2 can be transported upward again to the oxic zone, where both the sulphide and iron then can become oxidised (Schippers and Jørgensen 2002; Rickard and Luther 2007). This brief overview provides only a sketchy picture of the iron and sulphur cycling in marine sediments. In addition to these direct interactions between iron and sulphur, there are also links to the nitrogen cycle (e.g. nitrate can be used as an electron acceptor for both ferrous iron and sulphide), while also manganese can be involved in redox transformations of both iron and sulphur (Aller and Rude 1987; Aller 1994). Overall, the cycling of iron and sulphur in marine sediments is strongly intertwined and gives rise to a complex reaction network.

The complexity of sedimentary iron and sulphur cycling is further enhanced by the presence of fauna. Except for the oxygen minimum zones and permanently euxinic basins like the Black Sea and the Cariaco Basin, the present-day seafloor is mainly covered by oxygenated bottom waters. This availability of oxygen in combination with organic matter sinking down onto the sediment makes that most of the seafloor is inhabited and reworked by macrofauna (polychaetes, crustaceans, bivalves, etc.). These benthic fauna rework the sediment and influence sediment cycling in different ways: (1) by feeding, digestion, respiration and defecation, (2) by modifying the sediment structure and texture and (3) by inducing additional transport of solutes and solids, i.e. bioturbation (Meysman et al. 2006b; Middelburg and Levin 2009). Typically, these three mechanisms are active at the same time. During the feeding process, a fraction of organic matter is selectively retained for growth and metabolism, while the remaining fraction is repacked as faecal pellets and

excreted (thus affecting the structure of the sediment). The associated movement and burrowing generate additional physical and chemical heterogeneity within the sediment (Aller 2014). The term bioturbation generally refers to all types of biological reworking of sediments and involves two transport modes: the physical reworking of solid particles, i.e. bio-mixing, and the enhanced transport of solutes in the pore water, resulting from burrow flushing, i.e. bio-irrigation (Meysman et al. 2006a; Kristensen et al. 2012).

Bio-mixing is known to have a strong impact on geochemistry through the downward transport of reactive compounds, like reactive organic matter and iron- and manganese (oxyhydr)oxides, and the upward transport of reduced species to the sediment surface, like pyrite (Aller 1977). More specifically, bio-mixing actively transports reduced iron species into the oxic zone and reactive organic particles in the anoxic part of the sediment (Canfield et al. 1993; Aller 1994). This relocation of solid particles promotes the oxidation of organic matter via the anaerobic pathways such as dissimilatory iron reduction and sulphate reduction (Canfield et al. 1993; Thamdrup et al. 1994). Similarly, bio-irrigation introduces electron acceptors in the pore water at depth (e.g. oxygen, nitrate), while it removes electron donors (e.g. ferrous iron and sulphide) out of the sediment column (Aller and Aller 1998). In contrast to bio-mixing, the introduction of oxygen by bio-irrigation stimulates aerobic respiration at the expense of anaerobic pathways (Banta et al. 1999), while the removal of reduced species will limit the oxygen consumption for reoxidation (Banta et al. 1999; Renz and Forster 2014). Hence, bio-mixing and bio-irrigation appear to have a distinct—if not opposite—influence on the sediment geochemistry, but until now, this differential impact has not been given that much attention. Often, all the impacts of fauna on sediment geochemistry are conveniently aggregated under the umbrella term "bioturbation". The objective here is to open this "bioturbation black box" and to separately investigate the impact of bio-mixing and bio-irrigation on both the iron and sulphur cycling in marine sediments.

Benthic fauna hence have large impact on cycling of iron and sulphur, but the actual details and mechanisms are not very clear, as the interactions between the iron sulphur cycle and biological transport are many and complex. The iron and sulphur cycles in marine sediments are tightly coupled through a variety of biogeochemical pathways, while bio-mixing and bio-irrigation have a number of different impacts on the sediment geochemistry. In this paper, we have conducted a model analysis to elucidate the main impacts of bioturbation on the coupling between iron and sulphur. To this end, we developed an idealized model description for a bioturbated coastal sediment, which captures the dominant processes of the iron and sulphur cycling. Subsequently, we performed a sensitivity analysis, systematically changing the parameters associated with bio-mixing and bio-irrigation.

2 Materials and Methods

2.1 Conceptual Model of Redox Cycling in Bioturbated Sediments

The main purpose of our model study here is to describe the key interactions between bioturbation and iron (Fe) and sulphur (S) cycling. To this end, we have chosen to construct a simplified model of the geochemical cycling in bioturbated sediments. Purposely, this model includes only a selection of all biogeochemical processes that are known to

occur in coastal environments. A complex model with many parameters would make the interpretation of the results more difficult. Effectively, our aim was to construct a biogeochemical model of minimal complexity, which still is able to generate the two key features of Fe and S cycling in bioturbated sediments: (1) the formation of a suboxic zone and (2) the inclusion of an active redox cycle. The underlying conceptual model is illustrated in Fig. 1.

A **redox shuttle** refers to a redox transformation, where an intermediate redox compound continuously cycles between oxidised and reduced forms, and the oxidation and reduction steps take place in spatially segregated locations. In coastal bioturbated sediments, an iron-based redox shuttle is active in between the oxidation of free sulphide and the reduction of oxygen (Fig. 1). In a first step (the iron oxidation step), iron (oxyhydr)oxides (FeOOH) are formed, when ferrous iron comes (Fe^{2+}) into contact with oxygen (O_2) in the top millimetres of the sediment. In a second step (the iron reduction step), these iron (oxyhydr)oxides are used to oxidize free sulphide (H_2S) in the deeper sediment, thus producing again Fe^{2+}, which is transported upwards in the pore water or adsorbed onto sediment particles, thus making the cycle complete. Ferrous iron can also combine with H_2S to precipitate as iron sulphides (FeS), which is then mixed upwards by bio-mixing, thus providing another transport route of reduced iron to the upper sediment. The reduced and oxidised iron species thus function as intermediate redox species, shuttling electrons from sulphide to oxygen, hence the name redox shuttle.

A prime consequence of the iron-based redox shuttle in bioturbated sediments is the formation of a **suboxic zone**. Different definitions and interpretations of the term "suboxic zone" are used in the literature, and this has led to considerable confusion—see the review by Canfield and Thamdrup (2009). Here the suboxic zone is simply the depth layer where both O_2 and H_2S are undetectably low (Fig. 1). The oxygen penetration depth [OPD, operationally defined as the depth where (O_2) is below detection limit] and the sulphide appearance depth [SAD, operationally defined as the depth where (H_2S) is below detection

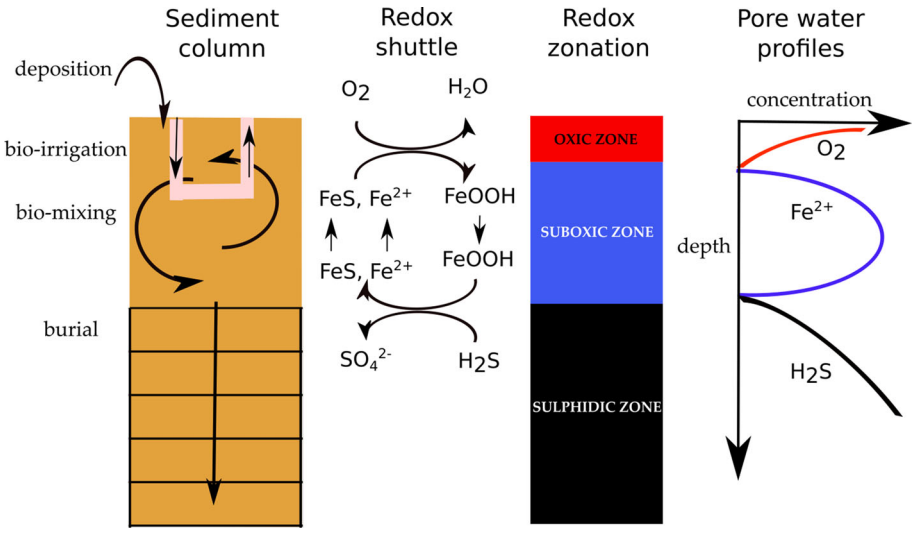

Fig. 1 Conceptual model of a sediment column (based on Aller 2014) impacted by bioturbation (bio-mixing + bio-irrigation) which shows the active redox shuttle, redox zonation and correspondent pore water profiles. See text for more details

limit] hence provide the upper and lower limits of the suboxic zone. This usage of the term suboxic zone does not make any inference about mineralization pathways that are acting. For example, sulphate reduction can take place at sizeable rates within the suboxic zone, although free sulphide is not present. However, if an iron-based redox shuttle is active, the suboxic zone will be characterized by the accumulation of ferrous iron. Accordingly, in bioturbated sediments with a sufficient iron input, one expects an oxic zone on top and a sulfidic zone below, separated from each other by a ferruginous suboxic zone (Fig. 1).

As noted above, bioturbation represents all faunal activities affecting the chemical composition of the sediment environment and generally involves two components (Meysman et al. 2006b; Kristensen et al. 2012): (1) the physical reworking of the sediment matrix through burrowing activities, which in general leads to enhanced solid particle transport, here referred to as bio-mixing, and (2) the enhanced transport of pore water solutes due to burrow ventilation activities, referred to as bio-irrigation. To investigate the differential effect of these bioturbation modes, we examine three model scenarios: (1) without bio-mixing and bio-irrigation, (2) only bio-mixing and (3) bio-mixing combined with bio-irrigation. When bio-mixing is introduced, the upper few centimetres of the sediment (where bioturbation is active) are homogenised. Bio-mixing only affects solid phase species and will transport organic carbon and iron (oxyhydr)oxides downward, thus stimulating dissimilatory iron reduction. At the same time, bio-mixing will also bring FeS upwards into the oxic zone, where it is oxidised back to FeOOH (Aller 1977; Berner and Westrich 1985). Accordingly, we expect that bio-mixing will lead to an intensification of the iron-based redox shuttle (Canfield et al. 1993; Thamdrup et al. 1994). Adding bio-irrigation to the model has two main consequences: solutes enriched in the pore water (Fe^{2+}, H_2S) will be transported out of the sediment into the overlying water column, while solutes that are depleted within the deeper pore water (O_2, SO_4^{2-}) will be introduced at depth from the overlying water (Aller and Aller 1998). Hence, the hypothesis is that the export of reduced Fe^{2+} and H_2S will prevent recycling of iron and sulphur and will thus decrease the iron-based redox shuttle. We will test these hypotheses by different model simulations. At the same time, we will test the hypothesis that FeS formation is crucial to sustain the iron-based redox shuttle, by performing simulations where the kinetic rate of FeS formation is artificially decreased or increased.

2.2 Biogeochemical Model Formulation

The depth profiles of solutes and solids in a cohesive marine sediment are described by the mass balance equations (Boudreau 1997; Meysman et al. 2005)

$$\begin{cases} \varphi \dfrac{\partial C_i}{\partial t} = \dfrac{\partial}{\partial z}\left(\varphi D_i \dfrac{\partial C_i}{\partial z} - \varphi v C_i\right) + \varphi \alpha(z)(C_{i,ow} - C_i(z)) + \displaystyle\sum_k v_{i,k} R_k \\ (1-\varphi)\dfrac{\partial S_i}{\partial t} = \dfrac{\partial}{\partial z}\left((1-\varphi) D_B(z) \dfrac{\partial S_i}{\partial z} - (1-\varphi) w S_i\right) + \displaystyle\sum_k v_{i,k} R_k \end{cases} \quad (1)$$

In this, C_i represents the concentration of a solute in the pore water, S_i is the concentration of a solid component, z is the depth into the sediment and φ the porosity. The model includes a set of transport processes that is characteristic for cohesive (i.e. low permeable) sediments impacted by fauna: (1) solute diffusion in the pore water, (2) downward advection due to sediment accumulation, (3) bio-mixing and (4) bio-irrigation. Pore water advection induced by bottom currents and waves, characteristic for permeable sediments, is not incorporated. Furthermore, concentration depth profiles are also influenced by a set

of biogeochemical reactions, where R_k represents the reaction rate and $v_{i,k}$ denotes the stoichiometric coefficient of the i-th species in the k-th reaction (the reaction set is detailed below).

The solute flux due to molecular diffusion and advection is described by Fick's first law (Fick 1855),

$$J_D = -\varphi D_i \frac{\partial C}{\partial z} + \varphi v C \tag{2}$$

where the effective diffusion coefficient is written as $D_i = D_0/\theta^2$, with D_0 the molecular diffusivity of the solute and $\theta^2 = 1 - 2\ln(\varphi)$ is a correction factor for sediment tortuosity (Boudreau 1996). The molecular diffusion coefficient D_0 is calculated as a function of the salinity S and temperature T using the R package CRAN: marelac (Soetaert et al. 2010a), which implements the constitutive relations listed in Boudreau (1997). The selected values for $S = 35$ and $T = 10$ °C represent mean annual values for temperate coastal environments (Table 1). To keep the model analysis tractable, sediment compaction is ignored, and so the porosity is taken to be constant with depth ($\varphi = 0.8$, a typical value for cohesive sediments in coastal environments). The absence of compaction also implies that the burial velocity of the pore water and the solid phase is identical. We fixed the sedimentation velocity at $v = w = 0.2$ cm year^{-1}, which represents a typical value for an accumulating coastal environments (the coastal range is 0.01–0.5 cm year^{-1} as in Boudreau 1997 and Mouret et al. 2009).

Following the conventional description (Boudreau 1997), bio-mixing is described as a diffusive process (see Meysman et al. 2010 for a theoretical justification)

Table 1 List of parameters included in the reactive transport model

Parameter	Depth profile		Symbol	Unit	Value
Salinity	Constant		S	–	35
Temperature	Constant		T_C	°C	10
Pressure	Constant		P	bar	1.013
pH	Constant		pH	–	7.5
Porosity	Constant		φ	–	0.8
Solid phase density	Constant		ρ_{sed}	g cm^{-3}	2.6
Sedimentation velocity	Constant	Porewater	v	cm year^{-1}	0.2
		Solid phase	w	cm year^{-1}	0.2
Bio-mixing	Sigmoïdal	Bio-mixing coefficient at the SWI	$D_{b,0}$	cm^2 year^{-1}	4
		Bio-mixing coefficient at infinity	$D_{b,\infty}$	cm^2 year^{-1}	0
		Mixing depth	x_L	cm	7.6
		Attenuation coefficient	x_{bm}	cm	2
Bio-irrigation	Exponential decrease	Bio-irrigation coefficient	α_0	year^{-1}	0
		Attenuation coefficient	x_{irr}	cm	3

The parameter values given are those used in the baseline simulation. A detailed description of the depth dependency of the bio-mixing and bio-irrigation coefficients is provided in the text

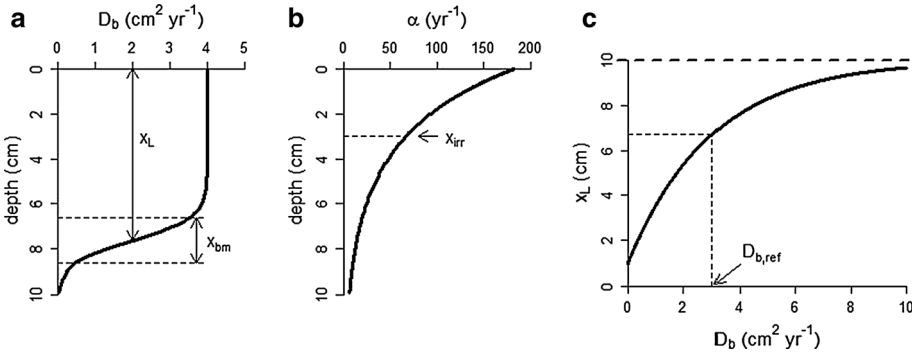

Fig. 2 Vertical depth profiles of **a** the bio-diffusivity coefficient ($D_{b,0}$), **b** the bio-irrigation coefficient (α_0) and **c** the dependency between the bio-diffusivity coefficient and the depth of the mixed layer (x_L) (see text for details)

$$J_b = -(1-\varphi)D_b\frac{\partial S}{\partial z} \tag{3}$$

Benthic fauna are dependent on food resources that settle from the overlying water, and so their ecology is tightly associated with the sediment–water interface (SWI). Accordingly, the most intense sediment reworking activity occurs in the top sediment layer and subsequently decreases with depth (Boudreau 1998). To describe this depth dependency, the bio-diffusivity (D_b) follows a sigmoidal depth profile (Fig. 2a)

$$D_b(z) = D_{b,0}\exp\left(-\frac{(z-x_L)}{0.25x_{bm}}\right)\Big/\left(1+\exp\left(-\frac{(z-x_L)}{0.25x_{bm}}\right)\right) \tag{4}$$

where $D_{b,0}$ is the bio-diffusivity at the SWI, x_L is the depth of the mixed layer and x_{bm} is an attenuation coefficient determining the width of the transition zone from mixed to unmixed sediment horizons. The bio-diffusivity remains constant up to a depth of $x_L - x_{bm}/2$, after which it decreases to zero at $x_L + x_{bm}/2$ (Fig. 2a).

Burrow structures can be flushed either actively or passively with overlying water, and the this bio-irrigational transport is typically described as a non-local exchange process, in which pore water parcels are exchanged with bottom water parcels (Boudreau 1984)

$$I_{\text{irr}}(z) = \alpha(z)(C_{ow} - C(z)) \tag{5}$$

The quantity $\alpha(z)$ represents the depth-dependent irrigation intensity, C_{ow} is the solute concentration of the bottom water, and $C(z)$ is the solute concentration at depth z. As in the case of bio-mixing, the bio-irrigation effect is generally most pronounced in the top layer of the sediment. However, the faunal activities that induce bio-mixing (e.g. locomotion and burrow construction) are different from those that underlie bio-irrigation (e.g. burrow ventilation), and so the depth dependency of both processes must not be the same. To account for the depth attenuation of bio-irrigation, we implemented the following exponential relation (Fig. 2b),

$$\alpha(z) = \alpha_0\exp\left(-\frac{z}{x_{\text{irr}}}\right) \tag{6}$$

where α_0 is the irrigation coefficient at the sediment–water interface (SWI), and x_{irr} is the depth attenuation coefficient of bio-irrigation (Fig. 2b).

Table 2 List of biogeochemical reactions included in the reactive transport model

Primary redox reactions			
R1	Aerobic respiration	AR_f	$\{CH_2O\}_f + O_2 \rightarrow HCO_3^- + H^+$
R2	Aerobic respiration	AR_s	$\{CH_2O\}_s + O_2 \rightarrow HCO_3^- + H^+$
R3	Dissimilatory iron reduction	DIR_f	$\{CH_2O\}_f + 4FeOOH + 7H^+ \rightarrow HCO_3^- + 4Fe^{2+} + 6H_2O$
R4	Dissimilatory iron reduction	DIR_s	$\{CH_2O\}_s + 4FeOOH + 7H^+ \rightarrow HCO_3^- + 4Fe^{2+} + 6H_2O$
R5	Sulphate reduction	SR_f	$\{CH_2O\}_f + \frac{1}{2}SO_4^{2-} \rightarrow HCO_3^- + \frac{1}{2}HS^- + \frac{1}{2}H^+$
R6	Sulphate reduction	SR_s	$\{CH_2O\}_s + \frac{1}{2}SO_4^{2-} \rightarrow HCO_3^- + \frac{1}{2}HS^- + \frac{1}{2}H^+$
Secondary redox reactions			
R7	Ferrous iron oxidation	FIO	$4Fe^{2+} + O_2 + 6H_2O \rightarrow 4FeOOH + 8H^+$
R8	Sorbed ferrous iron oxidation	SIO	$4X \equiv Fe^{2+} + O_2 + 6H_2O \rightarrow 4FeOOH + 8H^+$
R9	Canonical sulphur oxidation	CSO	$HS^- + 2O_2 \rightarrow SO_4^{2-} + H^+$
R10	Sulphide-mediated iron reduction	SIR	$HS^- + 8FeOOH + 15H^+ \rightarrow SO_4^{2-} + 8Fe^{2+} + 12H_2O$
R11	Iron sulphide oxidation	ISO	$FeS + \frac{9}{4}O_2 + \frac{3}{2}H_2O \rightarrow FeOOH + SO_4^{2-} + 2H^+$
Sorption/precipitation reactions			
R12	Iron sulphide precipitation	ISP	$Fe^{2+} + HS^- \rightarrow FeS + H^+$
R13	Iron sulphide dissolution	ISD	$FeS + H^+ \rightarrow Fe^{2+} + HS^-$
R14	Ferrous iron sorption	FIS	$Fe^{2+} \leftrightarrow X \equiv Fe^{2+}$

A distinction is made between mineralization reactions of organic matter ("primary redox reactions"), the subsequent reoxidation of mineralization products ("secondary redox reactions"), and sorption and precipitation reactions ("sorption/precipitation reactions"). The associated kinetic expressions are listed in Table 3

2.3 Biogeochemical Reaction Set

Together, the set of reactions ($n = 14$) in the model provides a parsimonious description of organic matter degradation linked to iron and sulphur cycling in coastal sediments (reaction set in Table 2; kinetic rate expressions in Table 3). As noted above, our goal was to construct a biogeochemical model of minimal complexity that can reproduce the iron-based redox shuttle in bioturbated sediments. As a result, the reaction set does not account for the cycling of manganese, nitrogen, phosphorus and carbonate minerals, as we believe that the inclusion of these cycles would not fundamentally change the operation of the iron-based redox shuttle.

Organic matter consists of two fractions: labile organic matter, which is easily degraded and has a high decay constant, and refractory organic matter, which is degraded at a slower rate (Westrich and Berner 1984). For each fraction, three mineralization pathways are included: aerobic respiration (AR), dissimilatory iron reduction (DIR) and sulphate reduction (SR) (Reactions R1–6; Table 2). Denitrification, methane formation and the reduction of manganese (hydr)oxides are not included, as these typically provide a smaller contribution to the total mineralization rate (Thamdrup 2000). The sequential usage of electron acceptors based on thermodynamic free energy gain (AR > DIR > SR) is implemented via a conventional limitation–inhibition formulation (Soetaert et al. 1996; Table 3).

The reduction of iron (oxyhydr)oxides (FeOOH) releases ferrous iron (Fe^{2+}) in the pore water, which can (1) adsorb onto solid phase particles (Thamdrup et al. 1994; Berg et al.

Table 3 List of kinetic rate expressions for the reactions included in the reactive transport model

	Reaction	Kinetic rate expression
M1	Mineralization fast organic matter ($R^f_{\min}$)	$(1-\varphi)k_f[CH_2O_f]$
M2	Mineralization slow organic matter ($R^s_{\min}$)	$(1-\varphi)k_s[CH_2O_s]$
R1	Aerobic respiration	$\frac{[O_2]}{[O_2]+K_{O_2}}R^f_{\min}$
R2	Aerobic respiration	$\frac{[O_2]}{[O_2]+K_{O_2}}R^s_{\min}$
R3	Dissimilatory iron reduction	$\frac{[FeOOH]}{[FeOOH]+K_{FeOOH}}\frac{K_{O_2}}{[O_2]+K_{O_2}}R^f_{\min}$
R4	Dissimilatory iron reduction	$\frac{[FeOOH]}{[FeOOH]+K_{FeOOH}}\frac{K_{O_2}}{[O_2]+K_{O_2}}R^s_{\min}$
R5	Sulphate reduction	$\frac{[SO_4^{2-}]}{[SO_4^{2-}]+K_{SO_4^{2-}}}\frac{K_{FeOOH}}{[FeOOH]+K_{FeOOH}}\frac{K_{O_2}}{[O_2]+K_{O_2}}R^f_{\min}$
R6	Sulphate reduction	$\frac{[SO_4^{2-}]}{[SO_4^{2-}]+K_{SO_4^{2-}}}\frac{K_{FeOOH}}{[FeOOH]+K_{FeOOH}}\frac{K_{O_2}}{[O_2]+K_{O_2}}R^s_{\min}$
R7	Ferrous iron oxidation	$\varphi k_{FIO}[O_2][Fe^{2+}]$
R8	Sorbed ferrous iron oxidation	$(1-\varphi)k_{SIO}[O_2][X\equiv Fe^{2+}]$
R9	Canonical sulphur oxidation	$\varphi k_{CSO}[O_2][HS^-]$
R10	Sulphide-mediated iron reduction	$(1-\varphi)k_{SIR}[FeOOH][HS^-]$
R11	Iron sulphide oxidation	$(1-\varphi)k_{ISO}[O_2][FeS]$
R12	Iron sulphide precipitation	$(1-\varphi)k_{ISP}\left(\frac{[Fe^{2+}][HS^-]}{[H^+]K^{SP}_{FeS}}-1\right)^{n_{ISP}}$
R13	Iron sulphide dissolution	$(1-\varphi)k_{ISD}[FeS]\left(1-\frac{[Fe^{2+}][HS^-]}{[H^+]K^{SP}_{FeS}}\right)^{n_{ISD}}$

All expressions are based on standard kinetic formulations used in sediment biogeochemical models (see text for details). The values of the kinetic constants are listed in Table 5

2003), (2) become reoxidised by oxygen (O_2) or (3) precipitate as iron sulphide (FeS) (Table 2). Similarly, sulphate reduction produces free sulphide (H_2S), which can be (1) reoxidised by O_2, (2) reoxidised by FeOOH or (3) precipitate as FeS (Reaction 9–10, 12–13; Table 2). FeS can be further oxidised in the presence of oxygen (Reaction R11; Table 2). The adsorption of Fe^{2+} is included as a reversible, linear adsorption process (R14; Table 2), where the concentration of adsorbed iron is in equilibrium at all times with the surrounding pore water, i.e. $[X\equiv Fe^{2+}] = K^{Fe^{2+}}_{ads}[Fe^{2+}]$, where $K^{Fe^{2+}}_{ads}$ is the adsorption constant (=696, a dimensionless value; Berg et al. 2003). This equilibrium formulation essentially assumes that adsorption proceeds much faster than the kinetics of the other reactions and also that the equilibrium is not influenced by environmental parameters (Berg et al. 2003).

The kinetic rate expressions of all reoxidation processes are described by standard second-order rate laws (Boudreau 1997; Table 3). The kinetics of dissolution and precipitation of FeS also follow the standard rate laws, where the reaction rate becomes dependent on the saturation state of the pore water (Van Cappellen and Wang 1996; Meysman et al. 2003; Table 3). The pH of the pore water is a controlling factor in the precipitation of FeS, but the pH is not explicitly modelled as a state variable, in order to reduce model complexity. Instead, we have adopted a constant depth profile with

pH = 7.5, which approximately means that the pore water is buffered by calcium carbonate at depth (Hofmann et al. 2008).

2.4 Numerical Solution

The model includes nine state variables in total: the concentrations of labile organic matter $[CH_2O]_f$, refractory organic matter $[CH_2O]_s$, dissolved inorganic carbon $[HCO_3^-]$, oxygen $[O_2]$, iron (oxyhydr)oxides [FeOOH], ferrous iron $[Fe^{2+}]$, sulphate $[SO_4^{2-}]$, free sulphide $[H_2S]$ and iron sulphide [FeS]. The open-source programming language R was used to implement a numerical solution procedure for the partial differential equations (Eq. 1), following the procedures of Soetaert and Meysman (2012) and Meysman et al. (2015). The spatial derivatives within the partial differential equations (Eq. 1) were expanded over the sediment grid using finite differences by using the R package CRAN:ReacTran (see Soetaert and Meysman 2012 for details). This sediment grid was generated by dividing the sediment domain (thickness $L = 10$ cm) into 200 sediment layers of variable thickness, with a higher resolution near the sediment–water interface where most intense geochemical cycling takes place (the first layer was 0.005 cm thick, and the thickness of the following layers increases with a factor 1.018). The resulting set of ordinary differential equations was integrated using the stiff equation solver routine "vode" (Brown et al. 1989) within the package CRAN:deSolve (Soetaert et al. 2010b). All model simulations were run for a sufficiently long time period (1000 year) to allow them to reach a steady state. The total inventories of pore water solutes were calculated as:

$$I_i = \varphi \int_0^L C_i(x)\mathrm{d}x \tag{7}$$

with L the depth of the sediment column (10 cm) and $C_i(x)$ the simulated concentration depth profile.

2.5 Model Parametrization

Our model analysis starts from a "baseline simulation", which is used as the starting point for all subsequent sensitivity analyses. The baseline simulation is meant to represent the iron-based redox shuttle, which is active in bioturbated coastal sediments. To properly distinguish the two effects of bioturbation, the baseline simulation only includes bio-mixing, and not bio-irrigation (see Sect. 4 below).

The parameter set for the baseline simulation was based on previous sediment studies at the Skagerrak site, an iron-rich site in the Baltic Sea, which is characterized by a large FeOOH influx and intense sulphate reduction (Canfield et al. 1993). In the baseline simulation, bio-mixing was described with a sigmoidal depth dependency ($D_{b,0} = 4$ cm^2 year^{-1}; $x_L = 7.6$ cm; $x_{bm} = 2$ cm). We further assumed that the flux of fast degradable organic carbon (OC_f) was 10 mmol C m^{-2} day^{-1}, and the flux of slow degradable organic carbon (OC_s) is half of that (Table 5), which are typical OC inputs for shelf sediments (Reimers and Suess 1983; Dale et al. 2015). The rain rate of reactive FeOOH was set at 0.33 mmol m^{-2} day^{-1}, which is in the range of estimates for the Skagerrak site, and there was no input of FeS from the overlying water column. The lower boundary conditions for all solid phase and solute species were set at a "no gradient" condition, implying that burial is the only process transporting material to deeper

sediments. This allows sediment to exit the model domain as fresh sediment is deposited on top. For solutes, the upper boundary conditions were set to concentrations typical for oxygenated bottom water: 0.28 mM of O_2 (100 % air saturation), 2.2 mM HCO_3^-, 28.2 mM of SO_4^{2-} and 0 for the reduced species Fe^{2+} and H_2S. All boundary conditions are summarized in Table 4.

The kinetic parameter set for the baseline simulation was based on previous modelling publications (Table 5). In natural seawater, the abiotic oxidation of ferrous iron with oxygen is a fast reaction with a half-life for Fe^{2+} in the range of 1–7 min (Millero et al. 1987a), the abiotic aerobic oxidation of sulphide has a half-life in the range of 1–2 days (Millero et al. 1987b) and the oxidation of FeS has a half-life of $\sim$5 days (Ahonen and Tuovinen 1991). When these reactions are microbially catalysed, they even proceed faster. For all three reactions, we assumed that microbial catalysis was dominant, and so we adopted high k values ($k = 10^7$ μmol^{-1} cm^3 year^{-1}), which implied that the reactions were transport controlled (i.e. any Fe^{2+}, H_2S or FeS transported into the oxic zone will be immediately oxidized). The terms "reaction control" and "transport control" relate to the behaviour of a chemical compound within the model. If the increase in a kinetic rate constant no longer influences a reaction rate, then the process is termed "transport controlled", meaning that it is limited by the transport supply pathways that are available in the model.

Poulton et al. (2004b) investigated the reactivity of iron (oxyhydr)oxide minerals with respect to reductive dissolution by free sulphide and showed that in essence two iron (oxyhydr)oxide pools can be distinguished in terms of reactivity (a high-reactive pool comprising freshly precipitated ferrihydrite, 2-line ferrihydrite and lepidocrocite and a less reactive pool consisting of goethite, magnetite and haematite). Here the model only includes the reactive iron (oxyhydr)oxide pool, and we assumed that the reactivity was similar to that of 2-line ferrihydrite (Burdige 2006). Poulton et al. (2004b) estimated a half-life ($t_{1/2} = \ln(2)/k$) of 12.3 h for this mineral at a free sulphide concentration of 1000 μM, which provides a k value of 494 μmol^{-1} cm^3 year^{-1} as used in the model here.

Finally, the kinetic constant of FeS precipitation was set at 10^4 μmol^{-1} cm^3 year^{-1}. This value can be compared to the value reported by Rickard (1995), who estimated a k value of 5×10^9 μmol^{-1} cm^3 year^{-1}. For reasons of numerical stability, we chose a lower k value. However, as FeS precipitation is transport limited above 10^4 μmol^{-1}

Table 4 Boundary conditions used in the reactive transport model

Species	UBC	Value	Unit
Solids			
OC_f	FF	365	μmol cm^{-2} year^{-1}
OC_s	FF	183	μmol cm^{-2} year^{-1}
FeS	FF	0	μmol cm^{-2} year^{-1}
FeOOH	FF	12	μmol cm^{-2} year^{-1}
Solutes			
O_2	FC	0.28	μmol cm^{-3}
DIC	FC	2.2	μmol cm^{-3}
HS^-	FC	0	μmol cm^{-3}
SO_4^{2-}	FC	28.2	μmol cm^{-3}
Fe^{2+}	FC	0	μmol cm^{-3}

UBC upper boundary condition, *FF* fixed flux, *FC* fixed concentration. All lower boundary conditions were set at no gradient

Table 5 Parameter values for the kinetic constants included in the reactive transport model

Constant	Symbol	Unit	Value	Reference
Organic matter reduction				
Decay constant fast degradable organic matter	k_f	$year^{-1}$	10	a
Decay constant slow degradable organic matter	k_s	$year^{-1}$	0.1	b
Monod constant oxygen consumption	K_{O_2}	$\mu mol\ cm^{-3}$	0.001	c, d
Monod constant dissimilatory iron reduction	K_{FeOOH}	$\mu mol\ cm^{-3}$	10.4	e
Monod constant sulphate reduction	$K_{SO_4^{2-}}$	$\mu mol\ cm^{-3}$	0.9	d
Oxidation reactions				
Canonical sulphide oxidation	k_{CSO}	$\mu mol^{-1}\ cm^3\ year^{-1}$	10^{+7}	d
Sulphide-mediated iron reduction (oxyhydr)oxides	k_{SIR}	$\mu mol^{-1}\ cm^3\ year^{-1}$	494	f
Iron sulphide oxidation	k_{ISO}	$\mu mol^{-1}\ cm^3\ year^{-1}$	10^{+7}	d
Ferrous iron oxidation	k_{FIO}	$\mu mol^{-1}\ cm^3\ year^{-1}$	10^{+7}	d
Sorbed ferrous iron oxidation	k_{SIO}	$\mu mol^{-1}\ cm^3\ year^{-1}$	10^{+7}	–
Iron sulphide reactions				
Iron sulphide precipitation	k_{ISP}	$\mu mol\ cm^{-3}\ year^{-1}$	10^{+4}	d
Iron sulphide dissolution	k_{ISD}	$year^{-1}$	3	d
Kinetic exponent iron sulphide precipitation	n_{ISP}	–	1	d
Kinetic exponent iron sulphide dissolution	n_{ISD}	–	1	d
Saturation constants				
Equilibrium constant ferrous iron sorption	$K_{ads}^{Fe^{2+}}$	–	696	g
Saturation constant iron sulphide	K_{FeS}^{SP}	$\mu mol\ cm^{-3}$	3160	h

All parameters are expressed per bulk volume of sediment

References: a: (Katsev et al. 2006); b: (Fossing et al. 2004); c: (Van Cappellen and Wang 1996); d: (Meysman et al. 2015); e: (Meysman et al. 2003); f: (Poulton et al. 2004a, b); g: (Berg et al. 2003); h: (Rickard 2006)

$cm^3\ year^{-1}$ (see Sect. 3 below), and increase in the k value above 10^4 will give no appreciable difference in model output.

2.6 Model Sensitivity Analysis

The sensitivity analysis examined three separate aspects: (1) sensitivity to bio-mixing, (2) sensitivity to bio-irrigation and (3) sensitivity to FeS precipitation. The sensitivity of the model results towards bio-mixing was first illustrated by presenting two end-member cases: "weak bio-mixing" ($D_{b,0} = 1\ cm^2\ year^{-1}$; $x_L = 3.6$ cm; $x_{bm} = 2$ cm) and "strong bio-mixing" ($D_{b,0} = 4\ cm^2\ year^{-1}$, $x_L = 7.6$ cm; $x_{bm} = 2$ cm). Note that the impact of bio-mixing is governed by two separate parameters: the intensity of mixing as represented by the bio-diffusivity, $D_{b,0}$, and the depth of the mixed layer, as represented by x_L (the width of the transition zone x_{bm} is of secondary importance and is not further adapted). In actual coastal sediments, the mixing intensity and mixing depth are correlated. Sediments that are subject to low mixing rates are typically inhabited by small fauna, which do not move deep into the sediment, and so sediment reworking is hence limited to a shallow surface layer (Taylor and Goldring 1993). With increasing animal size, the intensity of bio-mixing will increase, but simultaneously, the mixing depth will also increase. To account

for this interdependency, the mixing depth was made dependent on the bio-diffusivity by means of the following relation (Fig. 2c),

$$x_L = x_{L,0} + x_{L,\max}\left(1 - \exp\left(-D_{b,0}/D_{b,\mathrm{ref}}\right)\right) \quad (8)$$

where $x_{L,0}$ (=1 cm) is the minimum depth of bioturbation, $x_{L,\max}$ is the maximum mixing depth ($x_{L,0} + x_{L,\max} = 10$ cm; Boudreau 1998) and $D_{b,\mathrm{ref}}$ (=3 cm^2 year^{-1}) is a reference mixing intensity. This relation implies that the mixing depth first rapidly increases with a rising mixing intensity, but then saturates. This saturation response reflects that when the population density of the reworking fauna increases, the burrowing depth not necessarily increases. The advantage of implementing relation 8 is that the effect of bio-mixing could be investigated by only varying one single parameter: the surface bio-diffusivity coefficient $D_{b,0}$ was changed over the range 0.1–6 cm^2 year^{-1}, and each time, the associated mixing depth was calculated.

A second step was to add bio-irrigation to the baseline simulation and subsequently examine the sensitivity of the model towards variations in the bio-irrigation coefficient. Similarly as was done for the bio-diffusivity, two cases were investigated: "weak bio-irrigation" ($\alpha_0 = 0.1$ day^{-1}) and "strong bio-irrigation" ($\alpha_0 = 1$ day^{-1}), both with the same attenuation coefficient ($x_{\mathrm{irr}} = 3$ cm). While bio-mixing was kept at the baseline value ($D_{b,0} = 4$ cm^2 year^{-1}; $x_L = 7.6$ cm; $x_{bm} = 2$ cm), the impact of bio-irrigation was investigated by varying the surface bio-irrigation coefficient α_0 over the range 0–1 day^{-1} and calculating the associated steady state while keeping all other parameters constant. This means we vary from a situation with no bio-irrigation (but with bio-mixing) to a situation with very intensive burrow flushing (and keeping the same level of bio-mixing).

In a final step, the importance of the iron sulphide precipitation for the iron-based redox shuttle was evaluated. Two illustrative cases "slow FeS precipitation" ($k_{\mathrm{ISP}} = 10^{-2}$ μmol^{-1} cm^3 year^{-1}) and "fast FeS precipitation" ($k_{\mathrm{ISP}} = 10^{4}$ μmol^{-1} cm^3 year^{-1}) were investigated. In these simulations, bio-mixing was kept at its baseline value ($D_{b,0} = 4$ cm^2 year^{-1}) and bio-irrigation was set at an intermediate value ($\alpha_0 = 0.5$ day^{-1}). Subsequently, the kinetic constant of iron sulphide precipitation was varied from the "slow FeS precipitation" case to the "fast FeS precipitation" case (i.e. increased in five steps of each a factor 10).

3 Results

3.1 Baseline Simulation

The baseline simulation clearly reproduces the formation of a suboxic zone, which is defined here as a sediment horizon where both the O_2 and H_2S are absent. Operationally, the suboxic zone was delineated by verifying where the simulated concentration of O_2 and H_2S was <3 μM. All oxygen is consumed in the first 0.18 cm, while free sulphide only appears at 3.16 cm (Fig. 3a), thus generating a suboxic zone of 2.98 cm in the baseline simulation. The accumulation of Fe^{2+} in the pore water (up to a maximum of 0.12 mM) closely matches the extent of the suboxic zone: Fe^{2+} starts to appear right at the oxygen penetration depth and disappears where free sulphide starts to increase (Fig. 3a).

The suboxic zone also correlates with the depth zone over which FeOOH is consumed, while oppositely, FeS accumulates over the same depth (Fig. 3b). The depth profiles of FeOOH and FeS thus form a compensating mirror image, illustrating that FeOOH is

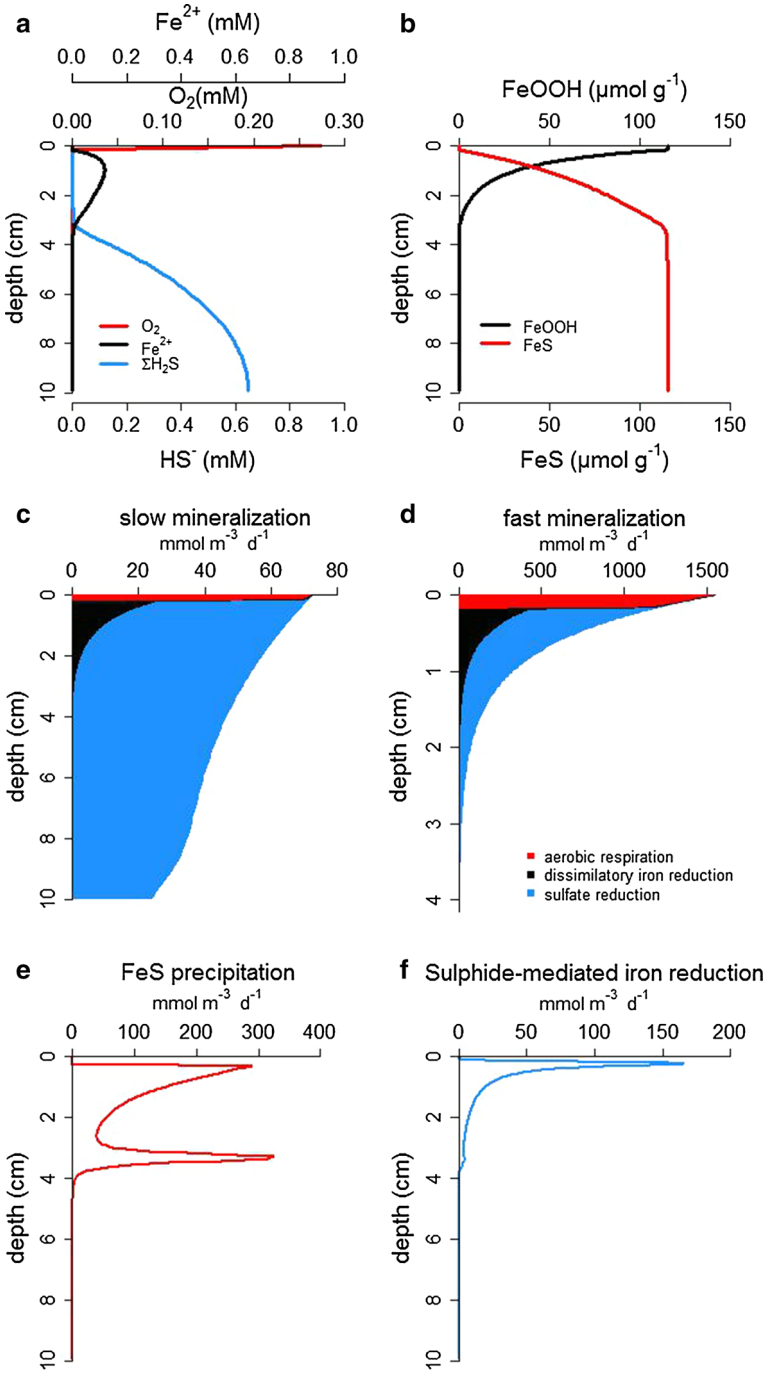
a
Fe2+ (mM)
0.0 0.2 0.4 0.6 0.8 1.0
O2(mM)
0.00 0.10 0.20 0.30
depth (cm)
0 2 4 6 8 10
O2
Fe2+
ΣH2S
0.0 0.2 0.4 0.6 0.8 1.0
HS- (mM)
b
FeOOH (µmol g-1)
0 50 100 150
depth (cm)
0 2 4 6 8 10
FeOOH
FeS
0 50 100 150
FeS (µmol g-1)
c
slow mineralization
mmol m-3 d-1
0 20 40 60 80
depth (cm)
0 2 4 6 8 10
d
fast mineralization
mmol m-3 d-1
0 500 1000 1500
depth (cm)
0 1 2 3 4
aerobic respiration
dissimilatory iron reduction
sulfate reduction
e
FeS precipitation
mmol m-3 d-1
0 100 200 300 400
depth (cm)
0 2 4 6 8 10
f
Sulphide-mediated iron reduction
mmol m-3 d-1
0 50 100 150 200
depth (cm)
0 2 4 6 8 10

◀**Fig. 3** Model output of the baseline simulation. **a** Concentration depth profiles of O_2, Fe^{2+} and HS^-, concentrations are expressed per unit volume of pore water. **b** Concentration depth profiles of FeOOH and FeS, concentrations are expressed per unit mass of solid phase. **c** Mineralization pathways of the slowly degradable organic matter. **d** Mineralization pathways of the fast degradable organic matter via aerobic mineralization, dissimilatory iron reduction and sulphate reduction. **e** Depth profile of the rate of FeS precipitation. **f** Depth profile of the rate of sulphide-mediated iron reduction. The reaction rates are expressed per unit volume of bulk sediment

converted to FeS in a one-to-one ratio. Note that in actual sediments, iron monosulphides (FeS) are further converted to pyrite (FeS_2), but this pyritization process is not explicitly included in the model. Hence, the "FeS" simulated should be interpreted as the total iron sulphide pool.

The mineralization of fresh organic matter (OM) is responsible for the largest part (10.0 mmol m^{-2} day^{-1}or 69 %) of the total mineralization rate (14.51 mmol m^{-2} day^{-1}; Table 6). While the high-reactive OM is consumed within the first 3 cm (Fig. 3d), the low-reactive OM is mineralized throughout the whole sediment depth of 10 cm (Fig. 3c). Sulphate reduction is the dominant mineralization pathway (10.24 mmol C m^{-2} day^{-1} or 71 %; Table 6), which is typical for coastal sediments (Jørgensen 1982; Burdige 1993). Aerobic respiration accounts for 17 % (2.45 mmol C m^{-2} day^{-1}; Table 6) of the total mineralization and is limited to the upper 0.18 cm, where oxygen penetrates by diffusion (note: the baseline simulation does not include bio-irrigation). Dissimilatory iron reduction (1.82 mmol C m^{-2} day^{-1} or 12 %; Table 6) shows a strong spatial overlap with sulphate reduction (Fig. 3c, d), which is because of the high parameter value for K_{FeOOH} (Table 5) adopted in the baseline simulation. This most likely reflects reality, as iron (oxyhydr)oxides in coastal sediments comprise a complex mixture of various iron minerals with different reactivities (Poulton and Canfield 2005). Only the most reactive iron (oxyhydr)oxides are preferentially consumed before sulphate, while others are consumed simultaneously with sulphate, thus providing an overlap between DIR and SR (Postma and Jakobsen 1996). Secondly, coastal sediments are characterized by substantial horizontal redox gradients and sediment heterogeneity, e.g. due to burrow networks, which allows different redox conditions and mineralization pathways to occur in the same depth layer (Aller 1977). In a one-dimensional representation, as in the diagenetic model employed here, such three-dimensional heterogeneity will show up as a depth overlap in mineralization pathways.

Two different reaction pathways are responsible for the removal of the free sulphide produced by sulphate reduction: the precipitation of iron sulphides (ISP) and sulphide-mediated iron reduction (SIR). The rate of canonical sulphide oxidation (CSO) is negligible, because O_2 and H_2S are spatially segregated due to the formation of a suboxic zone. Iron sulphide precipitation is the dominant pathway of sulphide removal (4.21 mmol S m^{-2} day^{-1}; Table 6), while sulphide-mediated iron reduction only presents a minor removal process (0.72 mmol S m^{-2} day^{-1}; Table 6). Both reactions do, however, have a similar depth profile (Fig. 3e–f), which is determined by the availability of H_2S, the primary reagent in both reactions. The subsurface maximum in ISP and SIR in the upper 2 cm follows from the mineralization of high-reactive organic matter (Fig. 3d), which produces H_2S via sulphate reduction. The second subsurface maximum in ISP occurs at 3.2 cm, i.e. near the sulphide appearance depth (Fig. 3a), where H_2S diffuses upward from deeper layers and comes in contact with Fe^{2+}, thus stimulating FeS precipitation.

Table 6 Summary of the model output of the baseline simulation (see text for detail)

Reaction rates			Fluxes		
Organic matter mineralization			SWI fluxes of solutes		
High-reactive organic matter	mmol C m^{-2} day^{-1}	10.0	Fe^{2+}	mmol m^{-2} day^{-1}	0.00
	%	69	HS^-	mmol m^{-2} day^{-1}	0.00
Low-reactive organic matter	mmol C m^{-2} day^{-1}	4.51	O_2	mmol m^{-2} day^{-1}	13.76
	%	31	SO_4^{2-}	mmol m^{-2} day^{-1}	0.44
Aerobic respiration	mmol C m^{-2} day^{-1}	2.45			
	%	17			
Dissimilatory iron reduction	mmol C m^{-2} day^{-1}	1.82			
	%	12			
Sulphate reduction	mmol C m^{-2} day^{-1}	10.24			
	%	71			
Secondary reactions			Burial fluxes of solids		
Ferric iron oxidation	mmol Fe m^{-2} day^{-1}	0.05	OC_f	mmol C m^{-2} day^{-1}	0.00
Sorbed iron oxidation	mmol Fe m^{-2} day^{-1}	8.81	OC_s	mmol C m^{-2} day^{-1}	0.49
Canonical sulphur oxidation	mmol S m^{-2} day^{-1}	0.18	FeOOH	mmol Fe m^{-2} day^{-1}	0.00
Sulphide-mediated iron reduction	mmol S m^{-2} day^{-1}	0.72	FeS	mmol Fe m^{-2} day^{-1}	0.33
FeS precipitation	mmol Fe m^{-2} day^{-2}	4.21	$X \equiv Fe^{2+}$	mmol Fe m^{-2} day^{-1}	0.00
FeS dissolution	mmol Fe m^{-2} day^{-2}	0.00			
FeS oxidation	mmol Fe m^{-2} day^{-2}	3.88			

SWI sediment–water interface

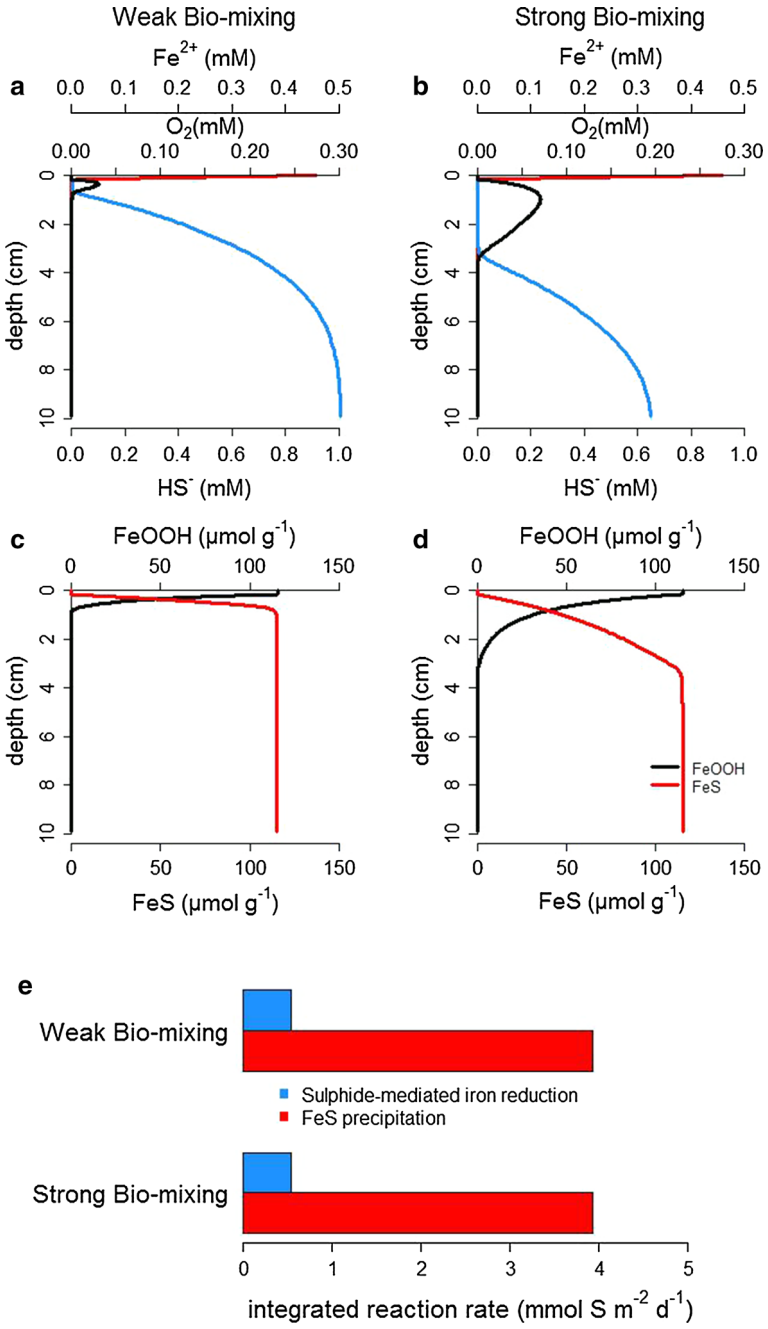

Fig. 4 Comparison of two intensities of bio-mixing "weak bio-mixing" at $D_{b,0} = 1$ cm^2 year^{-1} and "strong bio-mixing" at $D_{b,0} = 4$ cm^2 year^{-1}. **a**, **b** Concentration depth profiles of oxygen, Fe^{2+} and HS^-, concentrations are expressed per unit volume of pore water. **c**, **d** Concentration depth profiles of FeOOH and FeS, concentrations are expressed per unit mass of solid phase. **e** The depth-integrated rates of FeS precipitation and sulphide-mediated iron reduction

3.2 Model Response to Bio-mixing

The influence of bio-mixing was investigated by testing the bio-diffusivity coefficient $D_{b,0}$ over a range of 0.1–6 cm^2 $year^{-1}$ and simultaneously extending the depth of the mixed layer x_L from 1.0 to 8.8 cm (relation between $D_{b,0}$ and x_L as governed by Eq. 8). In these simulations, all other model parameters were kept at their baseline values (Tables 1, 5). Figure 4 shows the resulting depth profiles for the two end-member cases: weak bio-mixing ($D_{b,0} = 1$ cm^2 $year^{-1}$) and strong bio-mixing ($D_{b,0} = 4$ cm^2 $year^{-1}$). In addition, Fig. 5 shows the response of selected geochemical variables to gradually increased levels of bio-mixing, starting from a sediment with no faunal reworking.

The oxygen penetration depth (OPD) decreases from 2.9 to 1.8 mm with increasing bio-mixing (Fig. ES1). At the same time, the total O_2 uptake (TOU) decreases slightly (from 14.21 to 13.60 mmol m^{-2} day^{-1}; Table ES1). This decrease in the OPD at nearly constant TOU can be explained by a shift in the O_2 consumption from aerobic respiration to re-oxidation (Table 6). While aerobic respiration occurs uniformly throughout the oxic zone, re-oxidation is concentrated near the oxic-anoxic transition (i.e. near the OPD). Accordingly, with more intensive bio-mixing, the oxygen consumption becomes more localized near the OPD, thus straightening the O_2 depth profiles and reducing the OPD. In particular, with increased sediment reworking, more FeS is mixed into the oxic zone and this reacts quickly with O_2, thus reducing the OPD.

There is a clear impact of bio-mixing on the spatial segregation of O_2 and H_2S in the pore water. In the absence of bio-mixing, there is no suboxic zone (Fig. 5a). When moving from weak to strong bio-mixing, the width of the suboxic zone increases from 0.5 to 3.0 cm (Fig. 5a, b), while the subsurface accumulation of Fe^{2+} increases accordingly, and the inventory of H_2S decreases (Fig. 5c). Accordingly, more intensive bio-mixing causes a switch from sulphidic to ferruginous (Fe^{2+} rich) pore water conditions (Fig. 5c). More intensive (and deeper) bio-mixing also transports reactive FeOOH deeper into sediment and increases the FeOOH inventory (Fig. 5d). Oppositely, FeS is more easily mixed into the oxic zone, while its formation is delayed until deeper horizons (Fig. 4c, d), and as a result, more intensive bio-mixing decreases the inventory of FeS (Fig. 5d). Intriguingly, while FeS concentrations are lower, bio-mixing still slightly stimulates the precipitation of FeS at the expense of the direct interaction between sulphide and FeOOH (Fig. 4e).

Bio-mixing has also a pronounced impact on the relative importance of mineralization pathways (Fig. 5b). Dissimilatory iron reduction (DIR) and sulphate reduction are stimulated at the expense of aerobic respiration (SR increases from 25 to 71 %; DIR increases from 0 to 14 %; AR decreases from 74 to 14 %). Bio-mixing transports reactive organic matter deeper into the sediment, thus promoting anaerobic mineralization pathways over aerobic respiration, and at the same time, it increases the importance of re-oxidation reactions in the total oxygen consumption of the sediment. As already noted above, bio-mixing distributes FeOOH deeper in the sediment (Fig. 4c, d), and in this way, it promotes the production of Fe^{2+} via dissimilatory iron reduction (Thamdrup 2000) (Fig. 5b).

The inventory of H_2S displays a nonlinear response to increased bio-mixing (Fig. 5c). The H_2S inventory first increases to a maximum of 58 mmol m^{-2} at $D_{b,0} = 1$ cm^2 $year^{-1}$, after which it decreases again to vanishing small levels. At $D_{b,0} = 6$ cm^2 $year^{-1}$, there is no longer any free sulphide present in the whole sediment column (i.e. 10 cm). Hence, the strongest sulphidic pore water conditions are generated at intermediate bio-mixing intensities. The same nonlinear effect is also visible in the solid sulphur species (Fig. 5d), where FeS first slightly increases, but beyond $D_{b,0} = 0.5$ cm^2 $year^{-1}$, the FeS inventory starts to

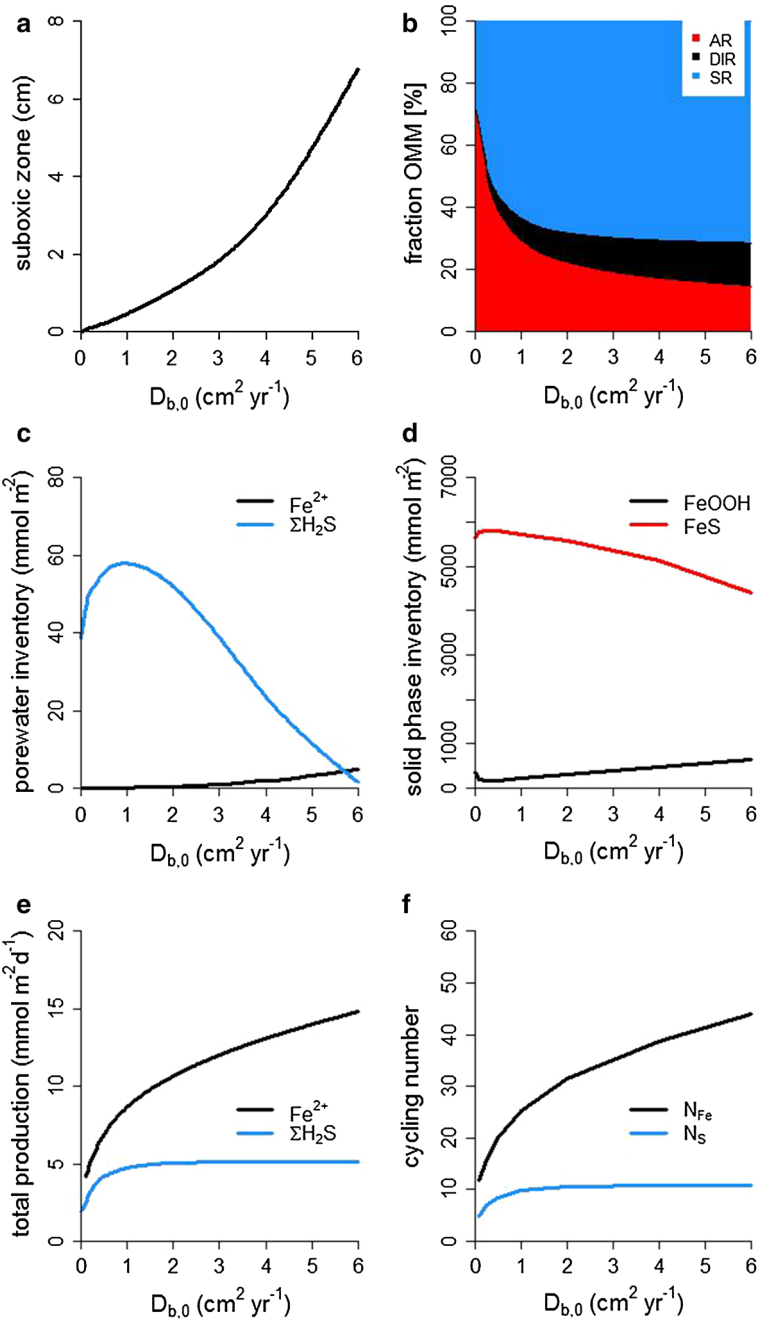

Fig. 5 Model sensitivity analysis of the bio-diffusivity coefficient ($D_{b,0}$ was varied from 0.1 to 6 cm^2 year^{-1}). **a** The width of the suboxic zone. **b** The relative importance of the different mineralization pathways (*AR* aerobic respiration, *DIR* dissimilatory iron reduction, *SR* sulphate reduction). **c** The porewater inventory of Fe^{2+} and HS^-. **d** The solid phase inventory of FeOOH and FeS. **e** The depth-integrated production rates of Fe^{2+} and HS^-. **f** The cycling number of Fe (N_{Fe}) and S (N_S), see text for detailed definitions

decline. This nonlinear effect arises from the dual effect of bio-mixing on FeS. With a small increase of $D_{b,0}$ (up to 0.5 cm^2 year^{-1}), the anaerobic mineralization pathways are stimulated and reduced Fe^{2+} and H_2S are formed. This stimulates the precipitation of FeS and thus supports a larger FeS inventory and a smaller FeOOH inventory (sequestration of Fe^{2+} as FeS prevents the reoxidation of Fe^{2+} to FeOOH). With stronger bio-mixing ($D_{b,0} > 0.5$ cm^2 year^{-1}), the stimulation of the anaerobic mineralization pathways is balanced by an intensified upward mixing and subsequent re-oxidation of FeS. As a result, the FeS inventory decreases, while the FeOOH inventory increases (Fig. 5d).

Overall, bio-mixing strongly stimulates the iron and sulphur cycling in the sediment and amplifies the iron-based redox shuttle (Fig. 5f). To quantitatively illustrate this, we can introduce the cycling number (N_{Fe}) of iron, which is defined as the ratio between the total production rate P_{FeOOH} of iron (hydr)oxides by re-oxidation and the total influx J_{FeOOH} of iron (hydr)oxides across the sediment–water interface.

$$N_{Fe} = \frac{P_{FeOOH}}{J_{FeOOH}} \tag{9}$$

In essence, the cycling number expresses the number of times an iron atom is internally recycled between oxidised and reduced forms, before it is buried as FeS (if FeOOH is directly converted into FeS and buried, then $N_{Fe} = 0$). A similar cycling number is defined for the sulphur cycle, where now the internal production of sulphate through reoxidation is compared to the external influx of sulphate across the SWI.

$$N_S = \frac{P_{SO_4^{2-}}}{J_{SO_4^{2-}}} \tag{10}$$

When bio-mixing is low ($D_{b,0} = 0.1$ cm^2 year^{-1}), the cycling numbers of both iron ($N_{Fe} = 12$) and sulphur ($N_S = 4.8$) are low. When fauna are absent, the recycling of Fe is driven by the upward diffusion of ferrous iron, its oxidation to FeOOH, and the subsequent downward transport of FeOOH by sediment accumulation (thus sustaining the $N_{Fe} = 12$).

When bio-mixing is introduced, the Fe cycling number rapidly increases fourfold to fivefold (Fig. 5f). The increased upward transport of adsorbed iron and FeS stimulates the oxidation of these compounds (Table 6), thus intensifying the production of FeOOH and increasing the N_{Fe}. The recycling of sulphur, however, responds slightly differently to increased bio-mixing. Compared to iron, the cycling number of sulphur is lower ($N_S = 4.8$) with low bio-mixing, as no solid phase transport is acting (as for FeOOH). Upon the introduction of bio-mixing, the cycling number of sulphur increases twofold to a high value of $N_S = 9.8$ at $D_b = 1$ cm^2 year^{-1} and only marginally increases thereafter (maximum $N_S = 11$) (Fig. 5f). The cycling number of S is strongly affected by the oxidation of FeS, because, in contrast to Fe, FeS is the only sulphur species affected by particle mixing. With increasing bioturbation, the oxidation of FeS strongly increases, after which it reaches a steady value (Table ES1), this behaviour is reflected in the N_S (Fig. 5f).

3.3 The Effect of Bio-irrigation

The effect of the bio-irrigation on sediment Fe and S dynamics was evaluated by increasing the bio-irrigation coefficient (α_0 from 0 to 1 day^{-1}), while keeping all other model parameters at their baseline values. Figure 6 shows two representative sets of depth profiles for sediments that are subject to weak bio-irrigation ($\alpha_0 = 0.1$ day^{-1}) and strong bio-irrigation ($\alpha_0 = 1$ day^{-1}). Figure 7 shows the response of selected geochemical variables

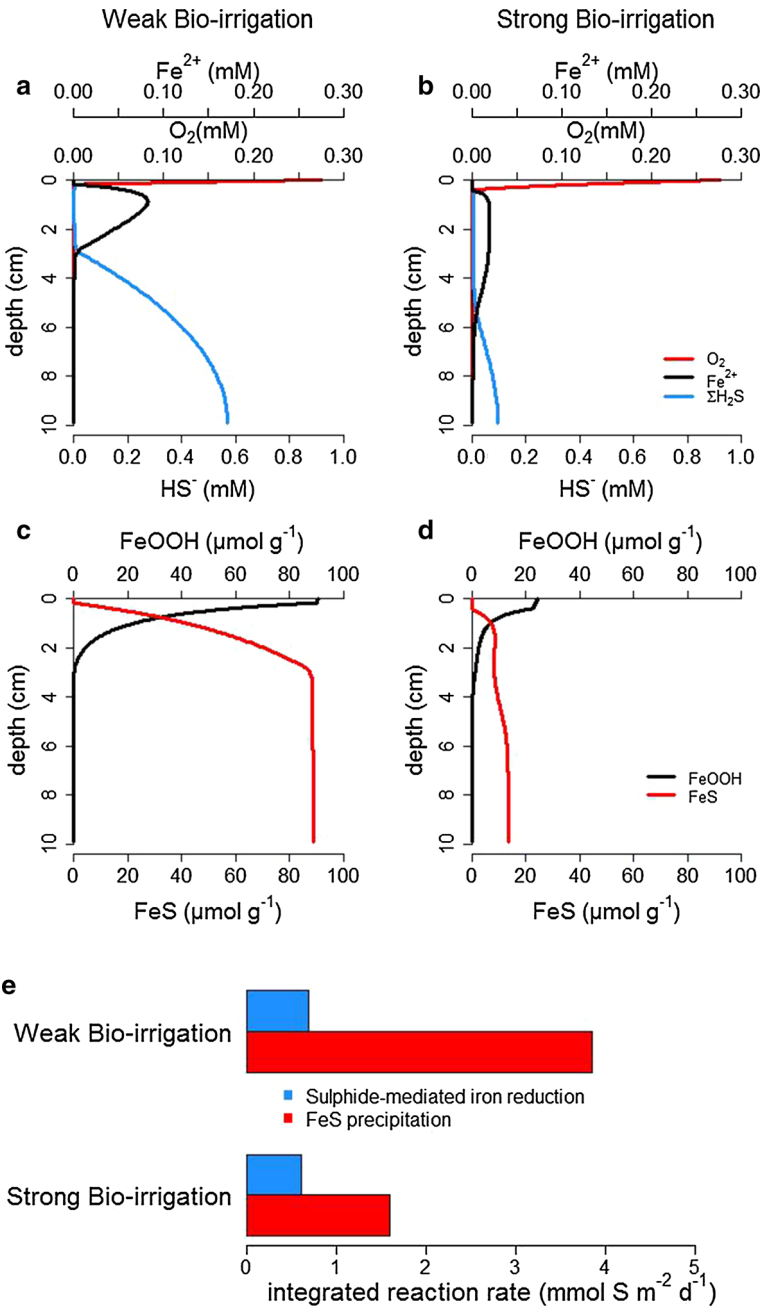

Fig. 6 Comparison of two intensities of bio-irrigation "weak Bio-irrigation" at $\alpha_0 = 0.1\ \text{day}^{-1}$ and "strong Bio-irrigation" at $\alpha_0 = 1\ \text{day}^{-1}$. **a**, **b** Concentration depth profiles of oxygen, Fe^{2+} and HS^-, concentrations are expressed per unit volume of pore water. **c**, **d** Concentration depth profiles of FeOOH and FeS, concentrations are expressed per unit mass of solid phase. **e** The depth-integrated rate of FeS precipitation and sulphide-mediated iron reduction

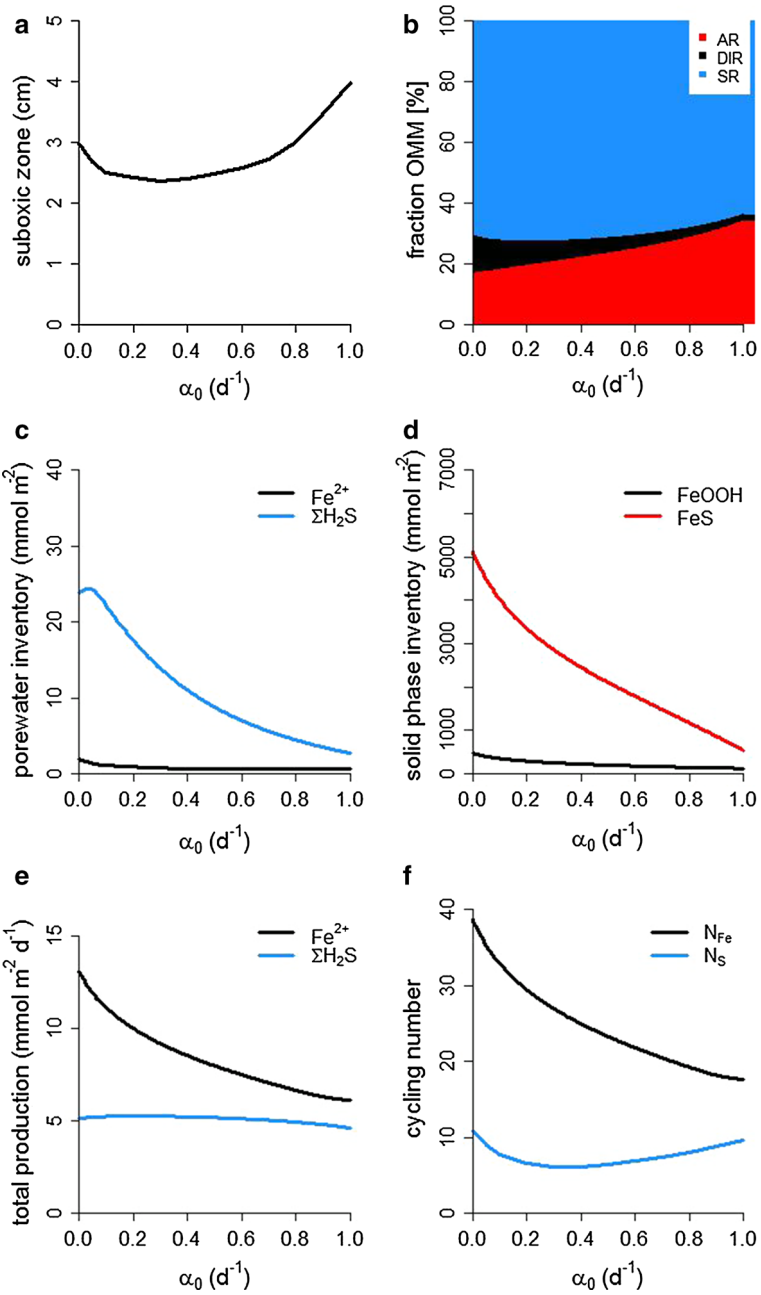

Fig. 7 Model sensitivity analysis for the bio-irrigation coefficient (α_0 was varied from 0 to 1 day^{-1}). **a** The width of the suboxic zone. **b** The relative importance of the different mineralization pathways (*AR* aerobic respiration, *DIR* dissimilatory iron reduction, *SR* sulphate reduction). **c** The porewater inventory of Fe^{2+} and HS^-. **d** The solid phase inventory of FeOOH and FeS. **e** The depth-integrated production rates of Fe^{2+} and HS^- **f** The cycling number of Fe (N_{Fe}) and S (N_S), see text for detailed definitions

to gradually increased levels of bio-irrigation, starting from a sediment with no bio-irrigation.

As expected, bio-irrigation increases the total O_2 uptake of the sediment and stimulates aerobic respiration (17.0–34.3 %) at the expense of sulphate reduction (70.5–63.6 %) and dissimilatory iron reduction (12.5–2.1 %) (Fig. 7b). At the same time, bio-irrigation increases the OPD (Fig. ES2) and stimulates aerobic respiration at the expense of O_2 consumption for re-oxidation.

Increasing bio-irrigation causes a decrease in the thickness of the suboxic zone (from 3.0 to 2.4 cm), after which the suboxic zone remains relatively constant, to gradually increase again at strong bio-irrigation ($\alpha_0 > 0.6$ day^{-1}) (Fig. 7a). The transport of reduced Fe^{2+} and H_2S out of the sediment and subsequent oxidation in the water column causes the initial decrease in the suboxic zone. This export prevents recycling of Fe^{2+} and formation of FeS, which decreases the total FeOOH and FeS inventory. The subsequent increase in the suboxic zone with intensified burrow flushing is a consequence of the introduction of more O_2 in the sediment. When O_2 is injected below the oxic layer depth, Fe^{2+}, H_2S and FeS are oxidised at depth. This leads to the formation of FeOOH in the deeper layers, which in its turn reacts with H_2S (either by reduction to Fe^{2+} and precipitation of FeS, or by direct sulphide-mediated iron reduction), and this sulphide removal leads to a deepening of the suboxic zone.

The increased efflux of Fe^{2+} across the sediment–water interface strongly affects the Fe cycling. By the removal of reduced Fe^{2+} from the sediment, internal recycling is prevented (the cycling number N_{Fe} drops by a factor $\sim$2; Fig. 7f) and the FeOOH inventory is reduced and the total Fe^{2+} production is decreased (Fig. 7d, e). In contrast, internal recycling of sulphur is less influenced (the cycling number N_S remains relatively constant around $\sim$8; Fig. 7f). This contrasting effect is due to the supply of SO_4^{2-}. While for iron, the SWI flux of FeOOH is fixed (as a boundary condition), and the influx of SO_4^{2-} consists of a diffusive flux and an irrigational flux, both of which depend on the SO_4^{2-} concentration in the pore water. As more bio-irrigation supplies more oxygen at depth, this will increase SO_4^{2-} production in the sediment column, which will lead to a decrease in SO_4^{2-} irrigational flux and thus an increase in N_S. This is a negative feedback mechanism, which will buffer strong changes in N_S. As less FeS is formed in the sediment (Fig. 7d), bio-irrigation substantially decreases the burial of iron sulphides (Table ES2).

3.4 Model Response to Kinetics of FeS Precipitation

The importance of iron sulphide precipitation (Table 2; Reaction R12) for the operation of the redox shuttle was studied by varying the kinetic constant of iron sulphide precipitation (k_{ISP}) over 6 orders of magnitude (from 10^{-2} to 10^4 μmol^{-1} cm^3 year^{-1}). This was done for a sediment with an intermediate level of bio-mixing ($D_{b,0} = 4$ cm^2 year^{-1}; $x_L = 7.6$ cm; $x_{bm} = 2$ cm) and bio-irrigation ($\alpha_0 = 0.5$ day^{-1}). Figure 8 shows representative sets of depth profiles for sediments that are subject to slow FeS precipitation ($k_{ISP} = 10^{-2}$ - μmol^{-1} cm^3 year^{-1}) and fast FeS precipitation ($k_{ISP} = 10^4$ μmol^{-1} cm^3 year^{-1}). Figures 9 and ES3 show the response of selected geochemical variables to gradually increased levels of k_{ISP}.

Three regimes can be distinguished: (1) no FeS precipitation ($k_{ISP} < 10^{-1}$), (2) reaction control (k_{ISP} between 10^{-1} and 10^{-3}) and (3) transport control ($k_{ISP} > 10^3$). The "no reaction" regime does not support a suboxic zone (Fig. 9a) and generates a high inventory of H_2S (15.4 mmol m^{-2}; Fig. 9c). Evidently, no FeS is present in the sediment column, and surprisingly, FeOOH is also present in low concentrations (Fig. 9d). This low FeOOH

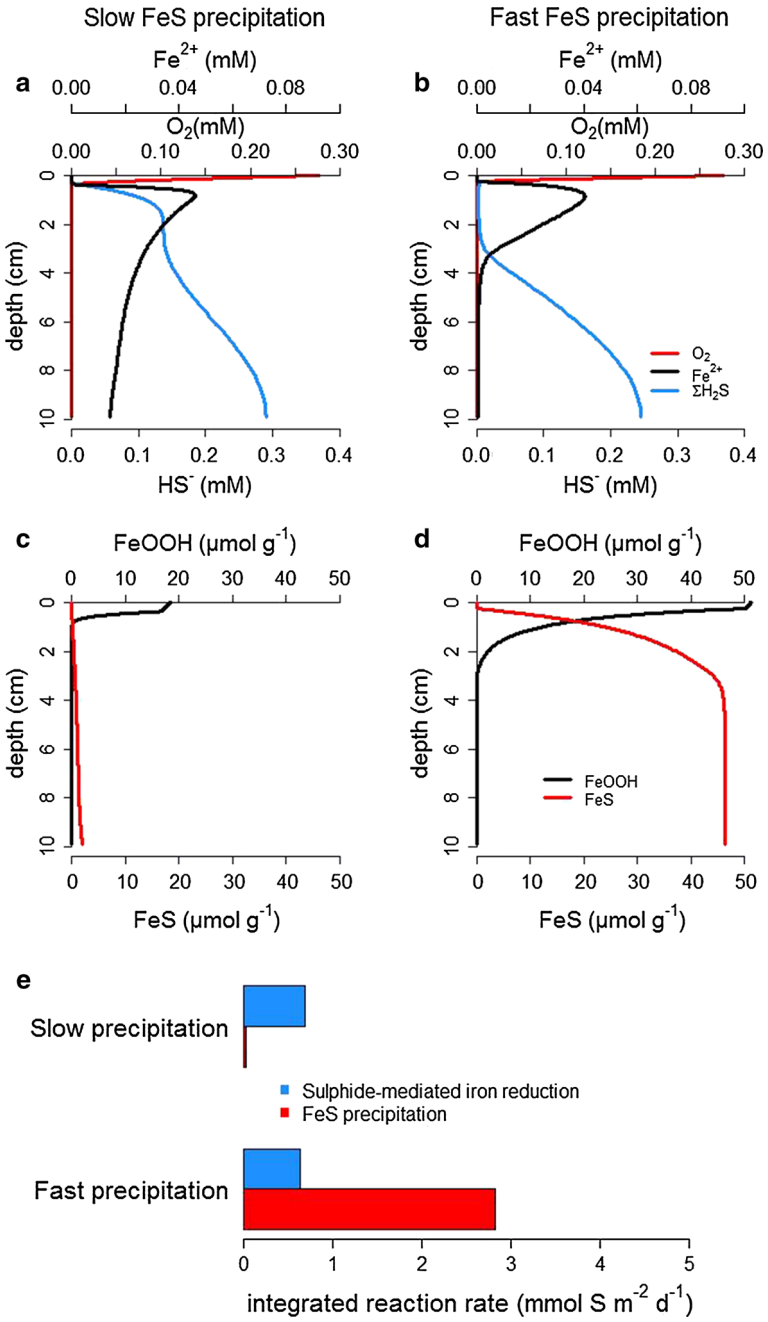

Fig. 8 Comparison of two intensities of FeS precipitation "slow FeS precipitation" at $k_{ISP} = 10^{-2}$ - μmol^{-1} cm^3 $year^{-1}$ and "fast FeS precipitation" at $k_{ISP} = 10^{+4}$ μmol^{-1} cm^3 $year^{-1}$. **a**, **b** Concentration depth profiles of oxygen, Fe^{2+} and HS^-, concentrations are expressed per unit volume of pore water. **c**, **d** Concentration depth profiles of FeOOH and FeS, concentrations are expressed per unit mass of solid phase. **e** The depth-integrated rates of FeS precipitation and sulphide-mediated iron reduction

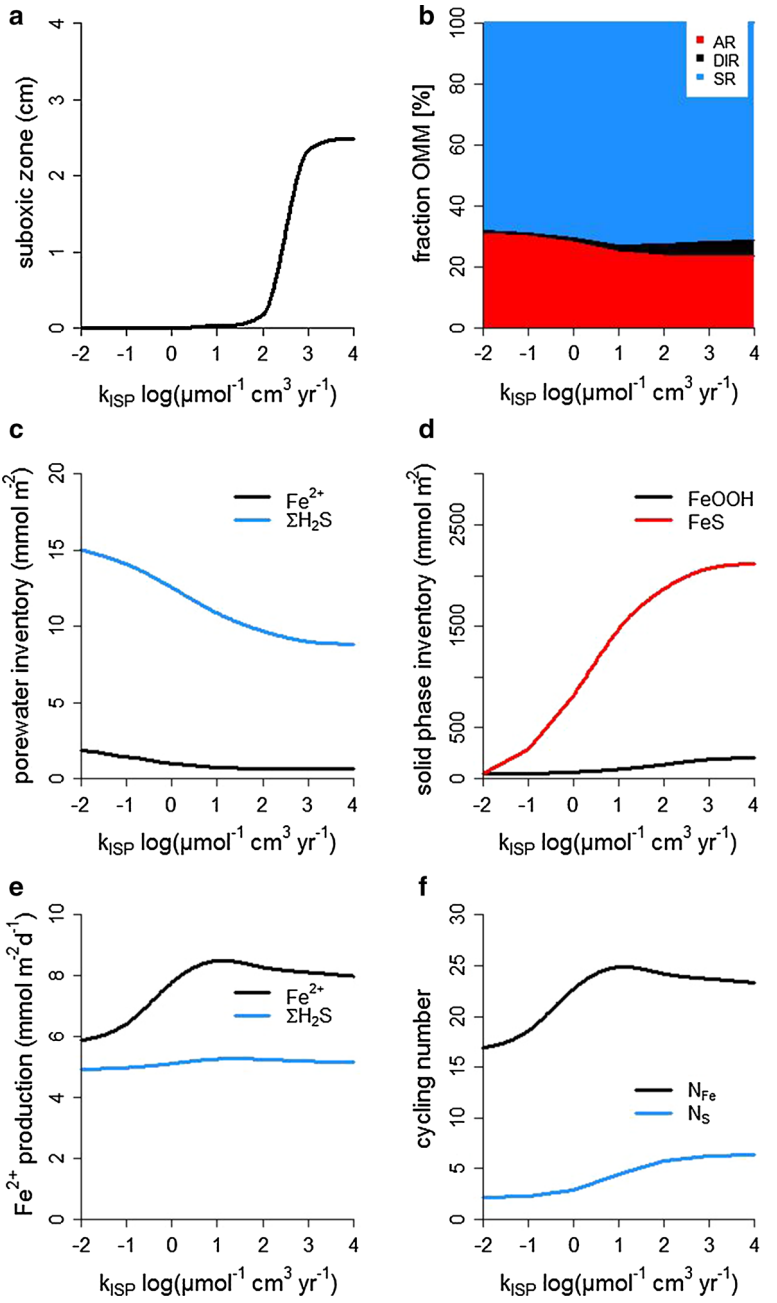

Fig. 9 Model sensitivity analysis for the kinetic parameter of FeS precipitation (k_{ISP} was varied from 10^{-2} to 10^{+4} μmol^{-1} cm^3 year^{-1}). **a** The width of the suboxic zone. **b** The relative importance of the different mineralization pathways (*AR* aerobic respiration, *DIR* dissimilatory iron reduction, *SR* sulphate reduction). **c** The porewater inventory of Fe^{2+} and HS^-. **d** The solid phase inventory of FeOOH and FeS. **e** The depth-integrated production of Fe^{2+} and HS^-. **f** The cycling number of Fe (N_{Fe}) and S (N_S), see text for detailed definitions

inventory leads to low dissimilatory iron reduction (0.3 %; Fig. 9b) and thus to a low Fe^{2+} production (5.9 mmol m^{-2} day^{-1}; Fig. 9e). The absence of FeS precipitation also limits the recycling of Fe (Fig. 9f). Furthermore, the inhibition of FeS precipitation also removes FeS burial as a possible export process for reduced Fe^{2+}. Hence, the irrigational efflux of Fe^{2+} across the sediment water interface increases with the decrease of k_{ISP} (Table ES3).

When the precipitation of FeS is increased (reaction control regime), free sulphide is removed and the suboxic zone deepens (Fig. 9a). The formation of FeS decreases the pore water inventories of Fe^{2+} and H_2S (Fig. 9c), stimulates the reoxidation of reduced Fe and S, and thus promotes the cycling of Fe and S (Fig. 9f). A further increase of k_{ISP} beyond the value of 10^3 μmol^{-1} cm^3 $year^{-1}$ does no longer affect the depth profiles of solids and solutes: the precipitation of FeS becomes transport limited (Note: the baseline simulation $k_{ISP} = 10^4$ μmol^{-1} cm^3 $year^{-1}$ lies in this regime).

4 Discussion

Previous studies have already suggested that bioturbation is a necessary driver to sustain strong iron and sulphur cycling in marine sediments (Canfield et al. 1993; Thamdrup et al. 1994; Raiswell and Canfield 2012), and our study confirms this. However, the effect of bioturbation involves two different components, i.e. bio-mixing and bio-irrigation (see Sects. 3.2 and 3.3), and these two components influence the sediment geochemistry in a different way. Bio-mixing affects the solid phase (Eq. 3), while bio-irrigation affects the pore water (Eq. 5). In discussions on marine sediment geochemistry, these two processes are often considered together, thereby implicitly assuming that they have a similar effect on the sediment geochemistry. However, our results here show that bio-mixing and bio-irrigation have a very differential impact on the Fe and S cycling in coastal sediments (Fig. 10).

4.1 Impact of Bioturbation on Suboxic Zone Formation and Fe^{2+} Accumulation

A suboxic zone is characterized by undetectable levels of both oxygen and sulphide (Berner 1981). The formation of a suboxic zone is very common in coastal sediments (Goldhaber and Kaplan 1974; Jørgensen 1982; Jørgenson and Nelson 2004; Burdige 2006) and can be formed by four distinct mechanisms (Aller 2014; Seitaj et al. 2015): (1) electrogenic sulphur oxidation by cable bacteria, which couple the reduction of oxygen near the sediment–water interface to the oxidation of sulphide in the deeper sediment layers via long-distance electron transfer (Nielsen et al. 2010; Pfeffer et al. 2012); (2) sulphide oxidation by motile, nitrate-accumulating filamentous bacteria (e.g. *Beggiatoa* and *Thioploca*) (Jørgensen and Gallardo 1999; Schulz and Jørgensen 2001; Sayama et al. 2005); (3) "mobile muds", which form on the Amazon inner shelf, where a muddy layer of >1 m is highly mobile and undergoes several deposition and resuspension cycles (Aller et al. 1986). In this case, sediment is sustained in a permanent state of transient diagenesis, with a continuous regeneration of reactive iron and manganese oxides; and (4) intensified iron cycling promoted by bio-mixing, in which iron acts as a redox shuttle between oxygen and sulphide (Canfield et al. 1993; Raiswell and Canfield 2012).

Our model simulations reveal in detail how a suboxic zone is generated in bioturbated sediments via the bio-mixing mechanism (Fig. 10). Essentially, the formation of a suboxic

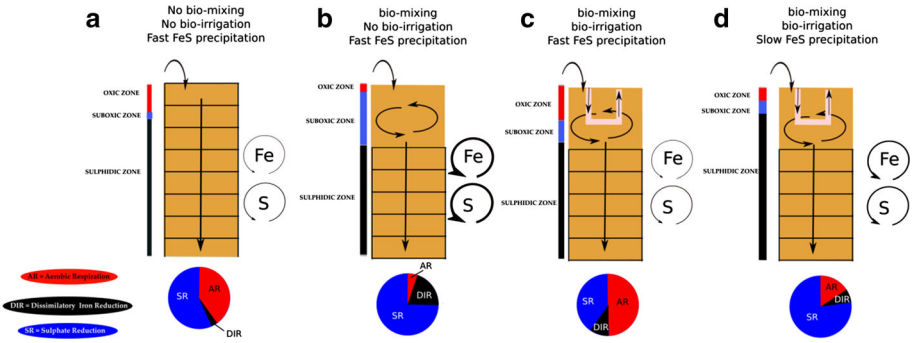

Fig. 10 Conceptual figure of the impact of bio-mixing, bio-irrigation and the kinetics of FeS precipitation on the redox cycling of Fe and S in the upper centimetres of a coastal sediment. The redox zoning, intensity of the Fe and S recycling and relative importance of the anaerobic mineralization pathways are highlighted (see text for more details). **a** The baseline situation (without bio-mixing, bio-irrigation and with fast precipitation of FeS), **b** situation with bio-mixing, **c** situation with bio-mixing and bio-irrigation, **d** situation with bio-mixing, bio-irrigation and slow kinetics of FeS precipitation

zone hinges on two processes: (1) the fast kinetics of FeS precipitation and (2) the presence of bio-mixing. Bio-mixing has two main effects: it introduces reactive FeOOH at depth, and conversely, it transports FeS and sorbed ferrous iron upwards to the oxic zone. This transport of solid phase iron compounds by bio-mixing forms the central "engine" of the redox shuttle between oxygen and sulphide (Fig. 1). Iron enters the sediment as insoluble FeOOH (Raiswell and Canfield 2012) and is transferred to the deeper layers via bio-mixing (Thamdrup 2000). While FeOOH is transferred downwards (past the oxygen penetration depth), dissimilatory iron reduction as well as sulphide-mediated iron reduction produces reduced Fe^{2+}. This ferrous iron precipitates quasi-instantaneously with H_2S, which is produced by sulphate reduction (Berner 1970) (Fig. 10). This mechanism leads to increasing concentrations of FeS and decreasing concentrations of FeOOH with depth and creates the separation between O_2 and H_2S (Fig. 3b). Simultaneously with the downward transport of FeOOH, the FeS produced is transported upwards into the oxic layer (Berner and Westrich 1985), in addition to Fe^{2+} that is sorbed onto various solid phases (Berg et al. 2003). When the sorbed Fe^{2+} and FeS come into contact with oxygen, they are rapidly reoxidised to FeOOH (Thamdrup et al. 1994). In the suboxic zone, all sulphides produced by sulphate reduction will be immediately captured by the Fe^{2+}, leading to ferruginous pore water conditions (Thamdrup et al. 1994). Below the mixed depth layer, the concentration of FeOOH is zero and the concentration of FeS remains constant (Fig. 2c, d) and sulphidic conditions prevail (Fig. 2a, b).

As noted above, the depth of the suboxic zone is highly dependent on the mechanism that forms the suboxic zone. Cable bacteria and nitrate-accumulating Beggiatoaceae typically generate a suboxic zone of 10–20 mm (Sayama et al. 2005; Seitaj et al. 2015), although recently cable bacteria have been shown capable of extending the suboxic zone down to 50 mm (van de Velde et al. accepted). The suboxic zone in sediments impacted by electrogenic sulphur oxidation is also characterized by the accumulation of Fe^{2+} in the pore water; cable bacteria strongly acidify the pore water and hence stimulate FeS dissolution (Risgaard-Petersen et al. 2012; Meysman et al. 2015). In contrast, *Beggiatoa* and *Thioploca* do not acidify the pore water, and hence, no FeS dissolution takes place, and so the pore waters of the suboxic zone do not show any Fe^{2+} accumulation. In both mobile muds and bio-mixed sediments, the reduction of reactive iron (oxyhydr)oxides is

responsible for the generation of the suboxic zone, and consequently, pore waters show accumulation of reduced Fe^{2+} up to where sediments are mixed (Aller 2014; Figs. 3 and 4). In the case of mobile muds, the suboxic zone can be extensive (>1 m) and depends on the depth to which the surface mud layer are mobilized and resuspended (this can exceed >1 m) (Aller et al. 1986). Finally, our simulations show that in the case of iron cycling promoted by bio-mixing, the extent of the suboxic zone depends on the depth affected by bio-mixing.

4.2 Impact of Bioturbation on Organic Matter Mineralization

Previously, it has been emphasized that an important effect of bio-mixing is the transport of organic carbon past the oxygen penetration depth, thus stimulating anaerobic pathways (Berner and Westrich 1985; Hines and Jones 1985). Our study reveals an additional mechanism that further enhances this effect: bio-mixing reduces the oxygen penetration depth (Fig. ES1) and so it is easier to transport organic matter in anoxic sediment horizons. The upward mixing of reduced FeS in the oxic layer decreases the OPD (Fig. ES1a), and this further reduces the oxygen consumption by aerobic respiration. One important question is whether this enhanced transport of organic matter below the OPD has any effect on the total mineralization rate. If the overall rate of organic matter degradation is independent of the electron acceptor, the stimulation of the anaerobic pathways would simply compensate for the reduction in aerobic respiration pathways, and the depth-integrated mineralization rate remains invariable. However, there is strong evidence that certain types of refractory matter are only degraded efficiently under oxic conditions (Kristensen et al. 1995). This would imply that bio-mixing decreases the total mineralization rate and thus promotes organic carbon preservation in marine sediments (Berner and Westrich 1985). In the simulations here, the kinetics of organic matter mineralization are not dependent on the electron acceptor, and so bio-mixing does not influence the total mineralization rate in our model simulations (Table ES1).

Foremost, bio-mixing and bio-irrigation have a pronounced differential effect on the partitioning between respiration pathways (Fig. 10). Overall, bio-mixing stimulates anaerobic mineralization and favours re-oxidation over aerobic respiration (Fig. 5b), while bio-irrigation does the opposite (Fig. 7b). Bio-irrigation stimulates aerobic respiration by introducing O_2 at depth (Jørgensen et al. 2005) and thus inhibits sulphate reduction or dissimilatory iron reduction. In addition, reduced species (Fe^{2+} and H_2S) are flushed out of the sediment and will be oxidized in the overlying water column rather than the sediment (Banta et al. 1999; Renz and Forster 2014). So as a result of bio-irrigation, less oxygen is utilized in reoxidation, and more oxygen becomes available for the mineralization of organic matter (Table ES2).

Overall, our study emphasizes that bio-mixing and bio-irrigation have an opposing effect on the mineralization pathways. Therefore, the particular faunal community present at any given site will be important, as it can influence the organic matter mineralization and associated redox cycling in a specific way. Some macrobenthos will induce strong bio-irrigation, while others are intensive bio-mixers, and some communities do both, dependent on the functional types of the bioturbation organisms that are present (François et al. 2002; Gilbert et al. 2007). Therefore, a proper understanding of the ecology of the bioturbating macrofauna at a given site seems important, as the particular transport regime induced by the fauna will be important to assess its impact on the geochemistry.

Since bioturbating macrofauna have a strong impact on mineralization pathways, they will inadvertently affect the microbial communities in the sediment. The upward mixing of

reduced compounds (i.e. FeS) likely stimulates autotrophic bacterial communities in the oxic zone, while the removal of H_2S and Fe^{2+} by bio-irrigation could promote chemo-autotrophy in the water column at the expense of similar communities in the sediment. Such anoxic plumes, induced by burrow ventilation, have been observed to leave the sediment in bio-irrigated coastal sediments (Volkenborn et al. 2010). Inversely, by making reactive organic carbon and iron (oxyhydr)oxides available in the absence of oxygen, anaerobic heterotrophic communities are stimulated in the anoxic sediment. One clear example of a bio-irrigation effect on microbial metabolism is the precipitation of iron (oxyhydr)oxides on the walls of burrows, which is due to the activity of autotrophic iron oxidisers that gain access to oxygen and Fe^{2+} by burrowing fauna (Kristensen and Kostka 2005).

4.3 Bioturbation and Sediment–Water Fluxes

Bio-mixing and bio-irrigation have a very different effect on the sediment–water fluxes. Bio-mixing strongly promotes the internal cycling of iron (oxyhydr)oxides and sulphate, but has hardly any effect on the fluxes across the sediment water interface of Fe^{2+} and H_2S (Table ES1). In theory, bio-mixing makes it easier for Fe^{2+} to escape the sediment. Bio-mixing promotes the internal cycling of iron (oxyhydr)oxides and stimulates the accumulation of Fe^{2+} in the pore water close to the sediment–water interface (thus facilitating a transfer to the overlying water). However, due to fast oxidation kinetics of Fe^{2+}, no iron can freely diffuse out of the sediment. For free sulphide, bio-mixing makes a transfer to the overlying water more difficult, as it creates a suboxic zone, thus pushing the appearance of free sulphide deeper into the sediment. As a result, the tendency of sulphide to escape by diffusion or sediment resuspension will be greatly reduced.

In contrast to bio-mixing, bio-irrigation has strong effects on the net exchange with the overlying water and increases the fluxes of Fe^{2+} and H_2S several fold (Table ES2). While the diffusive flux of H_2S and Fe^{2+} remain zero, the total efflux of H_2S increased from 0 to a maximum of 0.46 mmol m^{-2} day^{-1} at $\alpha_0 = 0.5$ day^{-1}, after which the input of O_2 in the sediment column decreases the rate of sulphate reduction strongly, and the release of H_2S in the pore water diminishes. The efflux of H_2S accordingly declines to 0.28 mmol m^{-2} day^{-1} at $\alpha_0 = 1$ day^{-1}. Ferrous iron shows a steady increase of Fe^{2+} efflux from 0 to 0.29 mmol m^{-2} day^{-1}.

While the incorporation of irrigation as non-local exchange term is valid in general (Boudreau 1984), some care should be taken when interpreting the flux results obtained from the simulations. The non-local exchange formulation assumes essentially that small parcels of pore water are directly exchanged with the overlying water and that no reoxidation occurs while transferring. Therefore, according to the non-local model of bio-irrigation, H_2S and Fe^{2+} would be transferred in reduced form to the overlying water, which is highly unlikely.

The diffusion of sulphide and ferrous iron from the anoxic surrounding sediment to the oxic burrow is slow when compared to the oxidation kinetics of both reduced solutes. This indicates that most of the Fe^{2+} and H_2S will be oxidized outside the burrow and will not be released in the overlying water (Meile et al. 2005). Nevertheless, anoxic plumes are released from sediment burrows (Volkenborn et al. 2010), showing that the oxygen concentration in the burrow is likely not high enough to capture all solutes and thus some reduced species will enter the overlying water.

When ferrous iron is oxidised inside the burrow environment, this will likely form colloidal or nanoparticulate ferric iron particles that remain in solution (Raiswell and

Canfield 2012). Hence, when burrows are flushed, these suspended forms iron will be transferred to the overlying water. Macrofauna thus can induce, via bio-irrigation, a substantial transfer of iron from the sediment to the overlying water. The redox state of the Fe that escapes the sediment will, however, depend on local oxygenation of the burrow.

The dissolved/suspended iron that is not taken up by phytoplankton will likely form colloïdal complexes that further aggregate and will rain down again on the sediment, thus forming a source of freshly precipitated, reactive iron to the sediment (Raiswell and Canfield 2012). However, these iron (oxyhydr)oxides will not rain down on exactly the same spot, as currents can transport them further away from the coast. This process can be cyclically repeated and can induce a shelf-to-basin shuttle of iron (Lyons and Severmann 2006), which has been shown to occur in the Black Sea (Wijsman et al. 2001) and the Baltic Sea (Reed et al. 2015) as well as open ocean settings near oxygen minimum zones (Scholz et al. 2014). The process stops when the iron reaches a deep basin, where the low content of reactive carbon allows the burial of iron (oxyhydr)oxides. Here, our model simulations confirm the earlier hypothesis that bio-irrigation can strongly promote the shelf-to-basin shuttle of iron (Raiswell and Canfield 2012), although further experimental verification of this hypothesis is required.

4.4 Bio-mixing and Bio-irrigation Exert a Differential Control on Fe and S Cycling

The biogeochemical cycles of Fe and S have been strongly connected throughout earth's history (Raiswell and Canfield 2012). The evolution of photosynthesis, which resulted in the Great Oxidation Event (GOE), strongly affected the earth surface chemistry (Canfield et al. 2013) and led to a more dynamic redox environment in the ocean with transitions between ferruginous, sulphidic and oxygenated conditions (Poulton et al. 2004a; Guilbaud et al. 2015). Eventually, the increased oxygen availability in the deep ocean allowed the evolution of animal life in marine sediments and associated the development of bioturbation (Canfield et al. 2007; Sperling et al. 2013; Chen et al. 2015), although the evolution of both ocean oxygenation and eukaryotes happened most likely simultaneously (Lenton et al. 2014).

Animals are "ecosystem engineers", and as such, they strongly shape the environment they inhabit as much as the environment influences them (Meysman et al. 2006b). In this aspect, the evolution of bioturbation could be an important factor for the biogeochemistry of both the sediments and water column after the so-called Cambrian explosion. Indeed, the dawn of animal life is suggested to be responsible for increasing the ocean sulphate concentration to modern levels of $\sim$28 mM (Canfield and Farquhar 2009). While the sulphate concentration in the Precambrian oceans increased as a response to increased oxidative weathering of sulphide minerals (Cameron 1982; Canfield et al. 2000), the further increase in sulphate concentration in the Phanerozoic oceans was most likely coupled to intensified reoxidation of sulphide in the sediments (Turchyn and Schrag 2004).

Via a model simulation, Canfield and Farquhar (2009) proposed that the evolution of bioturbation was the cause of this increased of sulphur recycling and thus was responsible for the increase in ocean sulphate concentration to modern levels near the end of the Phanerozoic. They introduced the ratio (x) of pyrite burial (J_{FeS}) over sulphate reduction (R_{SR}), calculated as $x = J_{FeS}/J_{FeS}$, and postulated that appearance of bioturbation decreased x by at least one order of magnitude (from 0.2 to 0.5 down to 0.033). If no free sulphide escapes the sediment, the burial of iron sulphide (J_{FeS}) should match the external input of sulphate ($J_{SO_4^-}$). Further, if free sulphide and sulphate are the only sulphur species

considered, the oxidation of sulphide to sulphate ($P_{SO_4^-}$) should match the internal production of sulphide by sulphate reduction (R_{SR}). As a result, the x-ratio defined by Canfield and Farquhar (2009) is essentially the inverse of our cycling number N_S (Eq. 9).

$$N_S = \frac{P_{SO_4^-}}{J_{SO_4^-}} = \frac{R_{SR}}{J_{FeS}} = \frac{1}{x} \tag{11}$$

The decrease in x in the model of Canfield and Farquhar (2009) then led to an increase in gypsum ($CaSO_4$) deposition and ocean sulphate concentration. In this model, the increase in sulphate concentration stimulates sulphate reduction, while the deposition of gypsum provides a cap that limits the increase in sulphate concentration (by generating and extra sulphur sink).

Our model results agree with the effect of the evolution of bioturbation as described by Canfield and Farquhar (2009), i.e. the evolution of bioturbation decreased the ratio of sulphide burial over sulphate reduction. In sediments without bioturbation, the x-ratio becomes 0.2 ($N_S = 4.8$; Fig. 5f), which is similar as proposed by Canfield and Farquhar, who suggested an x-ratio between 0.2 and 0.5 was likely. While in sediments with bio-mixing and bio-irrigation, this x-ratio attains a significantly lower value 0.09 ($N_S = 11$; Fig. 5f), about three times higher than estimated by Canfield and Farquhar ($x = 0.033$), illustrating that bioturbation strongly stimulates the reoxidation of sulphur relative to sulphur burial via iron sulphides.

However, as explained above, bioturbation involves two separate modes: bio-mixing and bio-irrigation (Kristensen et al. 2012). To illustrate the impact of both processes separately, we performed a dedicated model simulation. Starting from no bioturbation, we first gradually increased the intensity of bio-mixing, then introduced bio-irrigation, and gradually increased the intensity of bio-irrigation (Fig. 11). Although both processes decrease the burial ratio x (Fig. 11), the underlying reason is different. Turning on bio-mixing has no effect on the sulphide burial, but sulphate reduction is greatly enhanced as already discussed above (Fig. 5b). Oppositely, bio-irrigation has little effect on the

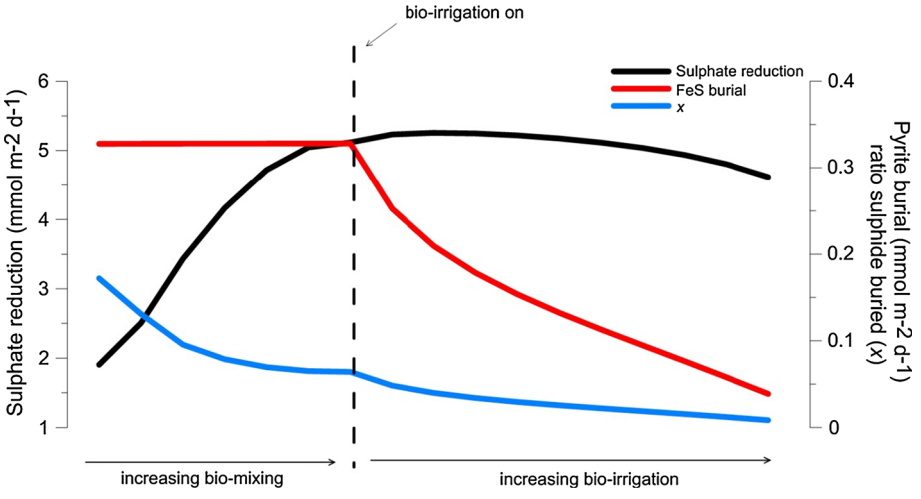

Fig. 11 Response of depth-integrated sulphate reduction rate, the burial flux of iron sulphide and the x-ratio to increasing bio-mixing (*left* of part of the figure) and increasing bio-irrigation (*right* part of the graph)

sulphate reduction rate, but flushes ferrous iron and sulphide out of the sediment, hence reducing iron sulphide formation and iron sulphide burial.

This different response of the iron and sulphur cycling to bio-mixing and bio-irrigation leads us to suggest that the effect of macrofauna on the sulphur chemistry was subtle, and perhaps, followed a two-step evolution. The first animals that evolved were likely small, did not burrow deep in the sediment, and presumably did not need to intensively flush their burrows. Gradually, the macrofauna grew bigger and simultaneously the bio-mixing intensity increased, but also the burrow systems extended deeper into the sediment. At some point, the bigger animals required more oxygen and thus needed to flush their burrows, which then initiated bio-irrigation. During the first step, the x-ratio of sulphide burial over sulphate reduction decreased rapidly due to the stimulation of sulphur recycling, while the sulphide burial remained constant. With the onset of bio-irrigation, the x-ratio decreased further, but this time sulphate reduction rate remained constant, while the pyrite burial decreased by the deep oxygenation of the sediment (Fig. 11). This would also mean that the first bioturbators did not have an effect on the sulphate concentration in the overlying water. Canfield and Farquhar (2009) already mentioned that the bioturbation intensity was probably low and the influence on the x-ratio unsure. Although the explanatory value of the sulphate model of Canfield and Farquhar is already strong, we propose that an adaptation of the model, with an inclusion of the differential behaviour between bio-mixing and bio-irrigation and a time dependent effect on x, could greatly improve the simulation of the evolution of sulphate concentrations in the Phanerozoic ocean (Fig. 11).

5 Conclusions

By means of a model sensitivity analysis, we have systematically explored the different impacts of two components of bioturbation, bio-mixing and bio-irrigation, on Fe and S cycling in marine sediments. This provides a number of insights. Firstly, we have shown that the formation of a suboxic zone and the operation of an iron-based redox shuttle is controlled by two key factors: the intensity of bio-mixing and the rapid kinetics of FeS formation. Biological mixing by macrofauna is needed to mix the reactive iron (oxyhydr)oxides, thus stimulating Fe^{2+} production in the sediment, while the low solubility of FeS and the fast precipitation kinetics of FeS efficiently use the Fe^{2+} to remove free sulphide from the pore water. The oxidation of sulphide by iron (oxyhydr)oxides alone (i.e. without FeS precipitation) is not strong enough to sustain a suboxic zone.

Furthermore, our model analysis confirms that bio-mixing is a necessary driver to sustain intense iron and sulphur cycling in marine sediments. The downward mixing of reactive organic particles and iron (hydr)oxides promotes anaerobic mineralization pathways, thus promoting the production of Fe^{2+} and free sulphide, while the upward mixing of reduced iron sulphide and adsorbed ferrous iron stimulates reoxidation of iron and sulphide, thus closing the redox shuttle.

However, it is important to recognize that the two components of bioturbation (bio-mixing and bio-irrigation) have contrasting effects on the iron an sulphur cycle, and thus, the impact of bioturbation on the sediment geochemistry depends on the lifestyle of the fauna that is locally present. Even though the extent to which the evolution of benthic fauna affected the geochemistry of the early earth is still largely unknown, it has already been recognized that the evolution of bioturbation has been a controlling factor for the

sulphate concentration in the water column. Also, the shelf-to-basin shuttle of Fe is most likely greatly stimulated by bio-irrigation. This strong dependence of the early diagenetic cycles of iron and sulphur on bioturbating animals in modern sediment shows that the dawn of bioturbation has been an important event in the evolution of the earth.

Acknowledgments The research leading to these results has received funding from the European Research Council under the European Union's Seventh Framework Programme (FP/2007–2013) through ERC Grant 306933 (FJRM) and was financially supported by Research Foundation Flanders (FWO Aspirant Ph.D. Fellowship to SVDV).

References

Ahonen L, Tuovinen OH (1991) Temperature Effects on Bacterial leaching of Sulfide minerals in shake flask experiments. Appl Environ Microbiol 57:138–145

Aller RC (1977) The influence of macrobenthos on chemical diagenesis of marine sediments. PhD thesis, Yale University, New Haven, Connecticut, 600 pp

Aller RC (1994) The sedimentary Mn cycle in Long Island Sound: its role as intermediate oxidant and the influence of bioturbation, O2, and Corg flux on diagenetic reaction balances. J Mar Res 52:259–295. doi:10.1357/0022240943077091

Aller RC (2014) Sedimentary diagenesis, depositional environments, and benthic fluxes. Treatise on geochemistry, 2nd edn. Elsevier Ltd., Amsterdam, pp 293–334

Aller RC, Rude PD (1987) Complete oxidation of solid phase sulfides by manganese and bacteria in anoxic marine sediments. Geochim Cosmochim Acta 52:751–765

Aller RC, Aller JY (1998) The effect of biogenic irrigation intensity and solute exchange on diagenetic reaction rates in marine sediments. J Mar Res 56:905–936. doi:10.1357/002224098321667413

Aller RC, Macking JE, Cox RTJ (1986) Diagenesis of Fe and S in Amazon inner shelf muds: apparent dominance of Fe reduction and implications for the genesis of ironstones. Cont Shelf Res 6:263–289

Banta GT, Holmer M, Jensen MH, Kristensen E (1999) Effects of two polychaete worms, Nereis diversicolor and Arenicola marina, on aerobic and anaerobic decomposition in a sandy marine sediment. Aquat Microb Ecol 19:189–204. doi:10.3354/ame019189

Berg P, Rysgaard S, Thamdrup B (2003) Dynamic modeling of early diagenesis and nutrient cycling. A case study in an artic marine sediment. Am J Sci 303:905–955. doi:10.2475/ajs.303.10.905

Berner RA (1970) Sedimentary pyrite formation. Am J Sci 268:1–23. doi:10.2475/ajs.268.1.1

Berner RA (1981) A new geochemical classification of sedimentary Environments. J Sediment Petrol 51:359–365

Berner RA, Westrich JT (1985) Bioturbation and the early diagenesis of carbon and sulfur. Am J Sci 285:193–206

Boudreau BP (1984) On the equivalence of nonlocal and radial-diffusion models for porewater irrigation. J Mar Res 42:731–735. doi:10.1357/002224084788505924

Boudreau BP (1996) The diffusive tortuosity of fine-grained unlithified sediments. Geochim Cosmochim Acta 60:3139–3142. doi:10.1016/0016-7037(96)00158-5

Boudreau BP (1997) Diagenetic models and their Implementation. Springer, Berlin

Boudreau BP (1998) Mean mixed depth of sediments: the wherefore and the why. Limnol Oceanogr 43:524–526

Brown PN, Byrne GD, Hindmarsh AC (1989) VODE, a variable-coefficient ODE solver. SIAM J Sci Stat Comput 10:1038–1051

Burdige DJ (1993) The biogeochemistry of manganese and iron reduction in marine sediments. Earth Sci Rev 35:249–284. doi:10.1016/0012-8252(93)90040-E

Burdige DJ (2006) Geochemistry of marine sediments. Princeton University Press, Princeton

Cameron EM (1982) Sulphate and sulphate reduction in early Precambrian oceans. Nature 296:145–148. doi:10.1017/CBO9781107415324.004

Canfield DE (1989) Reactive iron in marine sediments. Geochim Cosmochim Acta 53:619–632. doi:10.1016/0016-7037(89)90005-7

Canfield DE, Farquhar J (2009) Animal evolution, bioturbation, and the sulfate concentration of the oceans. Proc Natl Acad Sci 106:8123–8127

Canfield DE, Thamdrup B (2009) Towards a consistent classification scheme for geochemical environments, or, why we wish the term 'suboxic' would go away. Geobiology 7:385–392. doi:10.1111/j.1472-4669.2009.00214

Canfield DE, Jorgensen BB, Fossing H et al (1993) Pathways of organic carbon oxidation in three continental margin sediments. Mar Geol 113:27–40. doi:10.1016/0025-3227(93)90147-N

Canfield DE, Habicht KS, Thamdrup B (2000) The Archean sulfur cycle and the early history of atmospheric oxygen. Science 288:658–661. doi:10.1126/science.288.5466.658

Canfield DE, Poulton SW, Narbonne GM (2007) Late-neoproterozoic deep-ocean oxygenation and the rise of animal life. Science 315:92–95. doi:10.1126/science.1135013

Canfield DE, Ngombi-pemba L, Hammarlund EU et al (2013) Oxygen dynamics in the aftermath of the Great Oxidation of Earth' s atmosphere. Proc Natl Acad Sci 110:16736–16741. doi:10.1073/pnas.1315570110

Chen X, Ling H-F, Vance D et al (2015) Rise to modern levels of ocean oxygenation coincided with the Cambrian radiation of animals. Nat Commun 6:7142. doi:10.1038/ncomms8142

Dale AW, Nickelsen L, Scholz F et al (2015) A revised global estimate of dissolved iron fluxes from marine sediments. Global Biogeochem Cycles 29:1–17. doi:10.1002/2013GB004679.Received

Fick A (1855) Uber Diffusion. Ann Phys (N Y) 94:59–86

Fossing H, Berg P, Thamdrup B, Rysgaard S, Sørensen HM, Nielsen K (2004) A model set-up for an oxygen and nutrient flux model for Aarhus Bay (Denmark). NERI Technical Report No. 483, National Environmental Research Institute, Denmark, 65 pp

François F, Gerino M, Stora G et al (2002) Functional approach to sediment reworking by gallery-forming macrobenthic organisms: modeling and application with the polychaete Nereis diversicolor. Mar Ecol Prog Ser 229:127–136. doi:10.3354/meps229127

Gilbert F, Hulth S, Grossi V et al (2007) Sediment reworking by marine benthic species from the Gullmar Fjord (Western Sweden): importance of faunal biovolume. J Exp Mar Biol Ecol 348:133–144. doi:10.1016/j.jembe.2007.04.015

Goldhaber M, Kaplan I (1974) The sulfur cycle. In: Goldberg E (ed) The sea, 5th edn. Wiley-Interscience, New York

Guilbaud R, Poulton SW, Butterfield NJ et al (2015) A global transition to ferruginous conditions in the early Neoproterozoic oceans. Nat Geosci. doi:10.1038/NGEO2434

Hines ME, Jones GE (1985) Microbial biogeochemistry and bioturbation in the sediments of Great Bay, New Hampshire. Estuar Coast Shelf Sci 20:729–742

Hofmann AF, Meysman FJR, Soetaert K, Middelburg JJ (2008) A step-by-step procedure for pH model construction in aquatic systems. Biogeosciences 5:227–251. doi:10.5194/bgd-4-3723-2007

Jørgensen BB (1982) Mineralization of organic matter in the sea bed—the role of sulphate reduction. Nature 296:643–645

Jørgensen BB, Gallardo VA (1999) Thioploca spp.: filamentous sulfur bacteria with nitrate vacuoles. FEMS Microbiol Ecol 28:301–313

Jørgenson BB, Nelson DC (2004) Sulfide oxidation in marine sediments: geochemistry meets microbiology. In: Amend JP, Edwards KJ, Lyons TW (eds) Sulfur biogeochemistry past and present. The Geological Society of America, Inc., Bouldor, Colorado, pp 63–82

Jørgensen BB, Glud RN, Holby O (2005) Oxygen distribution and bioirrigation in Arctic fjord sediments (Svalbard, Barents Sea). Mar Ecol Prog Ser 292:85–95

Kristensen E, Kostka JE (2005) Macrofaunal burrows and irrigation in marine sediment: microbiological and biogeochemical interactions. Interact Between Macro Microorg Mar Sediments. doi:10.1029/CE060p0125

Katsev S, Sundby B, Mucci A (2006) Modeling vertical excursions of the redox boundary in sediments: Application to deep basins of the Arctic Ocean. Limnol and Oceanogr 51(4):1581–1593

Kristensen E, Ahmed SI, Devol AH (1995) Aerobic and anaerobic decomposition of organic matter in marine sediment: which is fastest? Limnol Oceanogr 40:1430–1437

Kristensen E, Penha-Lopes G, Delefosse M et al (2012) What is bioturbation? The need for a precise definition for fauna in aquatic sciences. Mar Ecol Prog Ser 446:285–302. doi:10.3354/meps09506

Lenton TM, Boyle RA, Poulton SW et al (2014) Co-evolution of eukaryotes and ocean oxygenation in the Neoproterozoic era. Nat Geosci 7:257–265. doi:10.1038/NGEO2108

Lovley DR (1991) Dissimilatory Fe(III) and Mn(IV) reduction. Microbiol Rev 55:259–287

Lyons TW, Severmann S (2006) A critical look at iron paleoredox proxies: new insights from modern euxinic marine basins. Geochim Cosmochim Acta 70:5698–5722. doi:10.1016/j.gca.2006.08.021

Meile C, Berg P, Van Cappellen P, Tuncay K (2005) Solute-specific pore water irrigation: implications for chemical cycling in early diagenesis. J Mar Res 63:601–621. doi:10.1357/0022240054307885

Meysman FJR, Middelburg JJ, Herman PMJ, Heip CHR (2003) Reactive transport in surface sediments. II. Media: an object-oriented problem-solving environment for early diagenesis. Comput Geosci 29:301–318. doi:10.1016/S0098-3004(03)00007-4

Meysman FJR, Boudreau BP, Middelburg JJ (2005) Modeling reactive transport in sediments subject to bioturbation and compaction. Geochim Cosmochim Acta 69:3601–3617. doi:10.1016/j.gca.2005.01.004

Meysman FJR, Galaktionov OS, Gribsholt B, Middelburg JJ (2006a) Bio-irrigation in permeable sediments: an assessment of model complexity. J Mar Res 64:589–627. doi:10.1357/002224006778715757

Meysman FJR, Middelburg JJ, Heip CHR (2006b) Bioturbation: a fresh look at Darwin's last idea. Trends Ecol Evol 21:688–695. doi:10.1016/j.tree.2006.08.002

Meysman FJR, Boudreau BP, Middelburg JJ (2010) When and why does bioturbation lead to diffusive mixing? J Mar Res 68:881–920

Meysman FJR, Risgaard-Petersen N, Malkin SY, Nielsen LP (2015) The geochemical fingerprint of microbial long-distance electron transport in the seafloor. Geochim Cosmochim Acta 152:122–142. doi:10.1016/j.gca.2014.12.014

Middelburg JJ, Levin LA (2009) Coastal hypoxia and sediment biogeochemistry. Biogeosciences 6:1273–1293

Millero FJ, Hubinger S, Fernandez M, Garnett S (1987a) Oxidation of H2S in Seawater as a function of temperature, pH, and ionic strength. Environ Sci Technol 21:439–443. doi:10.1021/es00159a003

Millero FJ, Sotolongo S, Izaguirre M (1987b) The oxidation kinetics of Fe(II) in seawater. Geochim Cosmochim Acta 51:793–801. doi:10.1016/0016-7037(87)90093-7

Mouret A, Anschutz P, Lecroart P et al (2009) Benthic geochemistry of manganese in the Bay of Biscay, and sediment mass accumulation rate. Geo Mar Lett 29:133–149. doi:10.1007/s00367-008-0130-6

Nielsen LP, Risgaard-Petersen N, Fossing H et al (2010) Electric currents couple spatially separated biogeochemical processes in marine sediment. Nature 463:1071–1074. doi:10.1038/nature08790

Pfeffer C, Larsen S, Song J et al (2012) Filamentous bacteria transport electrons over centimetre distances. Nature 491:218–221. doi:10.1038/nature11586

Postma D, Jakobsen R (1996) Redox zonation: equilibrium constraints on the Fe(III)/SO4-reduction interface. Geochim Cosmochim Acta 60:3169–3175. doi:10.1016/0016-7037(96)00156-1

Poulton SW, Canfield DE (2005) Development of a sequential extraction procedure for iron: implications for iron partitioning in continentally derived particulates. Chem Geol 214:209–221. doi:10.1016/j.chemgeo.2004.09.003

Poulton SW, Fralick PW, Canfield DE (2004a) The transition to a sulphidic ocean ~1.84 billion years ago. Nature 431:173–177. doi:10.1038/nature02863.1

Poulton SW, Krom MD, Raiswell R (2004b) A revised scheme for the reactivity of iron (oxyhydr)oxide minerals towards dissolved sulfide. Geochim Cosmochim Acta 68:3703–3715. doi:10.1016/j.gca.2004.03.012

Raiswell R, Canfield DE (2012) The iron biogeochemical cycle past and present. Geochem Perspect 1:1–232

Reed DC, Gustafsson BG, Slomp CP (2015) Shelf-to-basin iron shuttling enhances vivianite formation in deep Baltic Sea sediments. Earth Planet Sci Lett 1:1–11. doi:10.1016/j.epsl.2015.11.033

Reimers CE, Suess E (1983) The partitioning of organic carbon fluxes and sedimentary organic matter decomposition rates in the ocean. Mar Chem 13:141–168

Renz JR, Forster S (2014) Effects of bioirrigation by the three sibling species of *Marenzelleria* spp. on solute fluxes and porewater nutrient profiles. Mar Ecol Prog Ser 505:145–159. doi:10.3354/meps10756

Rickard D (1995) Kinetics of FeS precipitation: part 1. Competing reaction mechanisms. Geochim Cosmochim Acta 59:4367–4379. doi:10.1016/0016-7037(95)00251-T

Rickard D (2006) The solubility of FeS. Geochim Cosmochim Acta 70:5779–5789

Rickard D, Luther GW (2007) Chemistry of Iron Sulfides. Chem Rev 107(2):514–562. doi:10.1021/cr0503658

Risgaard-Petersen N, Revil A, Meister P, Nielsen LP (2012) Sulfur, iron-, and calcium cycling associated with natural electric currents running through marine sediment. Geochim Cosmochim Acta 92:1–13. doi:10.1016/j.gca.2012.05.036

Sayama M, Risgaard-petersen N, Nielsen LP et al (2005) Impact of bacterial NO3—transport on sediment biogeochemistry. Appl Environ Microbiol 71:7575–7577. doi:10.1128/AEM.71.11.7575

Schippers A, Jørgensen BB (2002) Biogeochemistry of pyrite and iron sulfide oxidation in marine sediments. Geochim Cosmochim Acta 66:85–92. doi:10.1016/S0016-7037(01)00745-1

Scholz F, Severmann S, Mcmanus J, Hensen C (2014) Beyond the Black Sea paradigm: the sedimentary fingerprint of an open-marine iron shuttle. Geochim Cosmochim Acta 127:368–380. doi:10.1016/j.gca.2013.11.041

Schulz HN, Jørgensen BB (2001) Big bacteria. Annu Rev Microbiol 55:105–137

Seitaj D, Schauer R, Sulu-gambari F et al (2015) Cable bacteria generate a firewall against euxinia in seasonally hypoxic basins. Proc Natl Acad Sci 112:13278–13283. doi:10.1073/pnas.1510152112
Soetaert K, Meysman F (2012) Reactive transport in aquatic ecosystems: rapid model prototyping in the open source software R. Environ Model Softw 32:49–60. doi:10.1016/j.envsoft.2011.08.011
Soetaert K, Herman PMJ, Middelburg JJ (1996) A model of early diagenetic processes from the shelf To abyssal depths. Geochim Cosmochim Acta 60:1019–1040
Soetaert K, Petzoldt T, Meysman FJR (2010a) marelac: Tools for Aquatic Sciences R package version 2.1
Soetaert K, Petzoldt T, Setzer RW (2010b) Package deSolve: solving initial value differential equations in R. J Stat Softw 33:1–25
Sperling EA, Halverson GP, Knoll AH et al (2013) A basin redox transect at the dawn of animal life. Earth Planet Sci Lett 371–372:143–155. doi:10.1016/j.epsl.2013.04.003
Taylor AM, Goldring R (1993) Description and analysis of bioturbation and ichnofabric. J Geol Soc London 150:141–148
Thamdrup B (2000) Bacterial manganese and iron reduction in aquatic sediments. In: Schink B (ed) Advances in microbial ecology, 16th edn. Luwer Academic/Plenum Publishers, New York, pp 41–84
Thamdrup B, Fossing H, Jorgensen BB (1994) Manganese, iron, and sulfur cycling in a coastal marine sediment, Aarhus Bay, Denmark. Geochim Cosmochim Acta 58:5115–5129
Turchyn AV, Schrag DP (2004) Oxygen isotope constraints on the sulfur cycle over the past 10 million years. Science 303:2004–2007. doi:10.1126/science.1092296
Van Cappellen P, Wang Y (1996) Cycling of iron and manganese in surface sediments: a general theory for the coupled transport and reaction of carbon, oxygen, nitrogen, sulfur, iron, and manganese. Am J Sci 296:197–243
Volkenborn N, Polerecky L, Wethey DS, Woodin SA (2010) Oscillatory porewater bioadvection in marine sediments induced by hydraulic activities of Arenicola marina. Limnol Oceanogr 55:1231–1247. doi:10.4319/lo.2010.55.3.1231
Westrich JT, Berner RA (1984) The role of sedimentary organic matter in bacterial sulfate reduction: the G model tested. Limnol Oceanogr 29:236–249. doi:10.4319/lo.1984.29.2.0236
Wijsman JWM, Middelburg JJ, Heip CHR (2001) Reactive iron in Black Sea Sediments: implications for iron recycling. Mar Geol 172:167–180. doi:10.1016/S0025-3227(00)00122-5
van de Velde S, Lesven L, Burdorf LDW et al. The impact of electrogenic sulfur oxidation on the biogeochemistry of coastal sediments: a field study. (accepted)
Zobell C, Rittenberg S (1948) Sulfate-reducing bacteria in marine sediments. J Mar Res 7:602–617